Uranus-Miranda Orbiter Design

WP3
C09

Attitude Determination and Control Sub-system

J. Alonso Garcia	5228530	K. S. Ganapathy	5331951
D. Gorovojs	5312450	M. Maximchuk	5208041
B. Mazur	5257980	D. Olimid	5260957
J. Oppelaar	5225450	S.J. Welters	5204968

Delft University of Technology

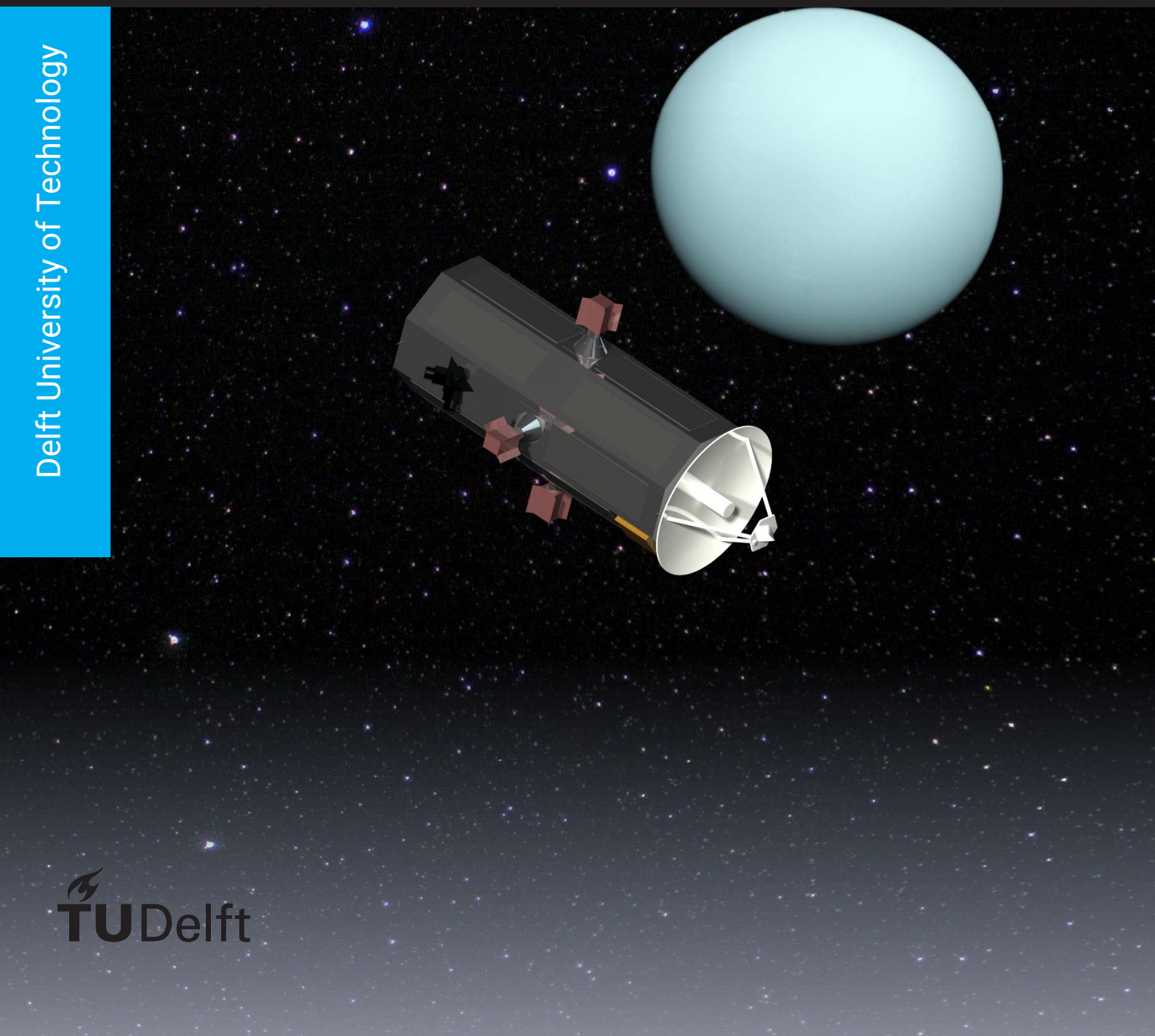

TUDelft

This page is intentionally left blank.

Uranus-Miranda Orbiter Design

Attitude Determination and Control Sub-system

by

Group C09

J. Alonso Garcia	5228530
K. S. Ganapathy	5331951
D. Gorovojs	5312450
M. Maximchuk	5208041
B. Mazur	5257980
D. Olimid	5260957
J. Oppelaar	5225450
S.J. Welters	5204968

Document type: Design Report
Date: October 18, 2021
Place: Delft, Netherlands
Course: AE2111-I Aerospace System Design
Project supervisor: Sorin Şeremet
Project coordinator: Dr. Ir. Woutijn J. Baars
Institution: Delft University of Technology
Revision: 1

TU Delft

Summary

Mankind's knowledge about the Gas Giants in our Solar system remains to this day limited. This is due to the limited amount of exploratory missions sent to these planets. Nevertheless, these celestial bodies contain essential information about the formation of our Solar system while housing a rich ecosystem of moons and natural satellites. The Uranus-Miranda Orbiter aims to fill this gap in the understanding of the outer planets by collecting scientific measurements of Uranus and its moon Miranda. The remoteness of these planets poses significant technological challenges, which qualifies this mission as a flagship project. With an expected launch in ten years, the design team is striving to come with a design which fulfils the ambitious objective of exploring the outskirts of our Solar system.

In this report the Attitude Determination and Control Sub-system is designed. Firstly, to better understand the expected performance of the sub-system, Chapter 2 starts with a study on the disturbance torques acting on the S/C throughout the duration of the mission. It was found that the disturbances can be distinguished into two types, environmental and internal. The environmental torques are composed of aerodynamic drag, solar pressure, gravity gradient and the magnetic field. The internal disturbances are caused by the misalignment between the centre of gravity and internal torques and forces. These include but are not limited to thruster misalignment, vibrations of the mechanical parts and sloshing of propellant. Furthermore, the total angular impulse per orbit is found to be 5.921 Nms, 9.87 Nms and 2.399 Nms along the roll, pitch and yaw axis respectively. This value was used to calculate the propellant mass, which resulted in 35.69 kg of propellant.

Secondly, in Chapter 3, an analysis of sensors and actuators used for the design is performed. Multiple technologies, both for sensors and actuators, are studied and analysed in this chapter. Four configurations for the final Attitude Determination and Control Sub-system are chosen and evaluated by means of a trade-off table. The optimal option contains one S3 sun sensor, three STAR-T3 star sensors, four GS-FOG50A fibre optic gyroscopes and two 3313A1 accelerometers for attitude determination and two CMG-12 control moment gyros, together with twelve 5N-HPGP thrusters for control. This setup provides the best balance between performance and power/weight budget, while fulfilling the requirements set.

Lastly, for the separate components to fulfil their task, they need to be properly integrated into the S/C. After careful considerations, the ADCS architecture illustrated in Figure 1 was decided upon. It illustrates the relations and interactions between numerous sub-system elements that are necessary for fully functioning S/C. Furthermore, power, propellant and data interfaces are considered, determining the paths between the Power Conditioning and Distribution Unit and the components. It is determined that ADCS sensors and actuators will communicate through an ADCS flight computer.

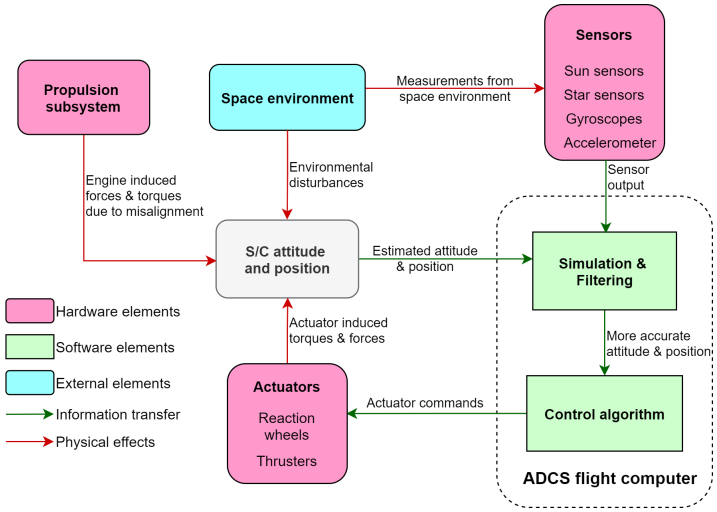

Figure 1: *ADCS architecture diagram*

Summarising, the second iteration of the design process for the Attitude Determination and Control Subsystem found a final design that is able to counteract the in-orbit disturbances and fulfils all requirements. To increase the performance of the sub-system, it is recommended to place the fuel tanks as close to the S/C's centre of mass as possible.

Contents

Nomenclature

ACC	Accelerometer
ADCS	Attitude Determination and Control Sub-system
CMG	Control Moment Gyro
COM	Centre Of Mass
COP	Centre Of Pressure
FOG	Fibre Optic Gyroscope
MW	Momentum Wheel
OCOP	Optical Centre Of Pressure
PCDU	Power Conditioning and Distribution Unit
RAM	Random Access Memory
RW	Reaction Wheel
S/C	Spacecraft
SNS	Sun Sensor
STS	Star Sensor
UMO	Uranus-Miranda Orbiter

β	Misalignment angle	rad
λ	Function of the magnetic latitude	-
μ	Gravitational parameter (GM)	km^3/s^2
ω	Angular velocity	rad/s
ϕ	Roll angle	rad
ψ	Yaw angle	rad
ρ	Atmospheric density	kg/m^3
ρ_p	Propellant density	kg/m^3
ρ_r	Reflectivity	-
τ	Torque	Nm
τ_{mt}	Main thruster misalignment torque	Nm
τ_d	Aerodynamic drag disturbance torque	Nm
τ_g	Gravity disturbance torque	Nm
τ_m	Magnetic disturbance torque	Nm
τ_s	Solar pressure disturbance torque	Nm
θ	Pitch angle	rad

ΔL	Angular impulse or change in angular momentum	Nms
$\dot{m}$	Mass flow	kg/s
Ω	Orbital mean motion	rad/s
a_{octagon}	Side length of octagon	m
B	Magnetic field	T
c	Speed of light	m/s
C_D	Drag coefficient	-
C_m	Centre of mass	m
D	Magnetic dipole moment	Am^2
d	Distance	m
$F_{\text{T, mt}}$	Main thruster thrust	N
F_a	Aerodynamic drag force	N
F_s	Solar radiation force	N
g_0	Standard gravitational acceleration of Earth	m/s^2
h	Angular momentum storage	Nms
$h_{\text{S/C}}$	Spacecraft height	m
I_{xx}	Mass moment of inertia around x-axis	kg m^2
I_{yy}	Mass moment of inertia around y-axis	kg m^2
I_{zz}	Mass moment of inertia around z-axis	kg m^2
J_s	Solar irradiance	W/m^2
L	Angular momentum	Nms
M	Magnetic dipole moment	Tm^3
m_{dry}	Dry mass of S/C	kg
m_{prop}	Propellant mass	kg
m_p	Propellant mass	kg
P_s	Solar pressure	Pa
R	Orbital radius	km
r_{cc}	Circumcircle radius of octagon	m
r_{mt}	Main thruster moment arm	m
r_{tank}	Propellant tank radius	m
r_d	Moment arm for aerodynamic drag	m
r_m	Moment arm	m
r_s	Moment arm for solar pressure	m
r_T	ADCS thurster moment arm	m

S	Surface area	m^2
s_{proj}	Projected side length of S/C	m
t_b	Burn time	s
T_o	Orbital period	s
v_{exh}	Exhaust velocity	m/s
v_o	Orbital velocity	m/s
V_p	Propellant volume	m^3

1

Introduction

Exploring the outer part of the solar system has always been a challenge due to the remoteness of the location. This explains why all the data available depicting Uranus is the one retrieved from the Voyager 2 mission, which performed a fly-by in 1986. However, it is believed that these outer planets contain essential information about the formation of our solar system.[1] The Uranus-Miranda orbiter is one the many S/C that aims to explore the Ice Giants in the next decade.

The aim of this report is to design down to the smallest detail the ADCS of the Uranus Miranda Orbiter (UMO). The velocity needed to be acquired by a S/C to reach Uranus is large, and the conditions to which the S/C will be subject to are extreme; thus, it becomes crucial to ensure that reliable data is collected after such an effort. This will be the task of the Attitude Determination and Control Sub-system (ADCS), which will ensure that the scientific instruments are properly oriented and that the part of the planet that wants to be investigated is in fact the one captured in the images. In the first report (WP1 [2]) some initial estimations were done, and more detailed calculations were made in the one that followed it (WP2 [3]). This report will ensure those decisions were correct and iterate the design of the S/C where needed.

This report begins by investigating the disturbance torques that will affect the S/C during the mission orbit and make recommendations on the design to minimise these in Chapter 2. Additionally the propellant mass needed for the ADCS will be calculated. In order to counteract those disturbances, actuators are sized in Chapter 3, together with the selection of sensors to provide attitude determination. This chapter finishes by presenting four different ADCS configurations. Lastly, a description of how will the ADCS be integrated with the rest of the S/C can be found in Chapter 4.

2

S/C Parameters and Disturbances

During the mission around Uranus, the S/C will experience several disturbances caused by various effects. Firstly, the geometric parameters of the S/C are presented in Section 2.1. Secondly, using the geometric parameters, the external disturbance torques caused by the atmosphere, gravitational attraction and magnetic field of Uranus, and the solar pressure from the Sun are presented in Section 2.2. Thirdly, the internal disturbances, which are effects due to errors and misalignments inside the S/C, are discussed in Section 2.3. Fourthly, in Section 2.4, using the torques caused by the disturbances the angular impulse and propellant mass for the ADCS are calculated and presented. Lastly, in Section 2.5, measures to reduce these disturbances are presented.

All calculations are made using the python scripts in Appendix B.

2.1. S/C Geometric Parameters and modes

Spacecraft coordinate system and reference frame

The origin of the coordinate system is defined as the position of the geometric centre of the S/C. This will be used for the calculations in this chapter. Additionally for the calculation made, a geodetic reference frame is used as illustrated in Figure 2.1[4]. Since the UMO orbits in a polar orbit, the lowest orbital inclination possible is 7.77°, which is the same as the the obliquity to orbit of Uranus.[5] This inclination was planned to be taken into account as well, but because of time constraints, it is not included in this study. The inclination used for the calculations is 0°, parallel to the orbital plane of Uranus and the Sun.

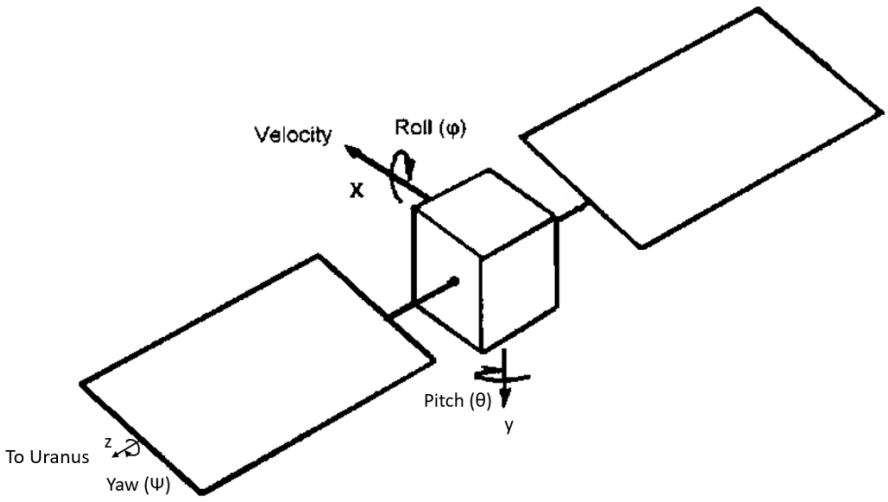

Figure 2.1: *Definition of reference frame, geodetic reference frame (original retrieved from [6])*

Centre of Mass

The centre of mass of the S/C is used to calculate the disturbance torques. Due to the currently unknown design of the spacecraft and the masses of the parts, the COM of the dry mass of the S/C is assumed to be at the geometric centre of the S/C. Designing a S/C with a COM at the geometric centre is essential to reduce the disturbance torques on a S/C. For the total S/C, the COM is computed using the dry mass and the propellant mass for station keeping. Additionally, according to the propellant tank configuration provided in [3], it is found that the distance between the origin and the centre of mass of the propellant tanks is 0.702 m below the origin. The propellant mass for station keeping varies throughout the mission, thus an average is

considered. In WP2[3], a propellant mass residual of 2% was considered. This results in the following values: initial propellant mass, $m_{\text{prop,i}} = 180.73 \cdot 1.2$ and final propellant mass, $m_{\text{prop,f}} = 180.73 \cdot 1.2 \cdot (1 - 1/1.02)$.[3] Using the location of centre of mass of propellant tank, the mass of the propellant, and the dry mass of the S/C, the centre of mass of the entire S/C can be found using Equation 2.1.[6]

$$r_x = \frac{m_{p,av} \cdot r_p}{m_{\text{dry}} + m_{p,av}} \tag{2.1}$$

Additionally, due to the assumption made that the centre of mass location of the dry mass of the S/C is at the geometric centre, an uncertainty is added. According to [7, p. 574], a centre of gravity uncertainty of 0.02 m is considered. Centre of mass of both mass values were calculated and an average was taken, this value is considered for all following calculations. This results in a final centre of mass array of: $C_m = [0.0649\,\text{m}, 0.02\,\text{m}, 0.02\,\text{m}]$.

Dimensions and Areas

The S/C is considered to be a regular octagonal prism, as in WP2[3]. The dimensions are presented in Table 2.1 and are used for all following calculations. The projected side length of the S/C is: $s_{\text{proj}} = a(1+\sqrt{2})$, using the geometry of the S/C. Due to the uncertainty of the S/C areas, due to sub-systems protruding the vehicle, a margin of 5% is added. Using Equation 2.2 and the margin, the final values are calculated, and are presented in Table 2.1.

$$\begin{aligned} S_x &= 2\sqrt{2} r_{\text{cc}}^2 \\ S_y &= s_{\text{proj}} \cdot h_{\text{SC}} \\ S_z &= S_y \end{aligned} \tag{2.2}$$

where

S_x = the frontal area of the S/C, in the yz-plane,
S_y = the projected area in the xz-plane,
S_z = the projected area in the xy-plane,
r_{cc} = the circumcircle radius of the octagon,
s_{proj} = projected side length of the S/C,

Table 2.1: *S/C geometrical parameters*

Category	**Unit**	**Parameters**	**Value**
Dimensions	[m]	Height ($h_{\text{S/C}}$)	8.235
	[m]	Circumcircle radius (r_{cc})	1.80
	[m]	Side length (a_{octagon})	1.378
	[m]	Projected side length (s_{proj})	3.327
Projected areas	[m^2]	S_x (yz-plane)	9.62
	[m^2]	S_y (xz-plane)	28.77
	[m^2]	S_z (xy-plane)	S_y
MMOI	[$kg\,m^2$]	I_{xx}	2334.34
	[$kg\,m^2$]	I_{yy}	10353.43
	[$kg\,m^2$]	I_{zz}	I_{yy}

Mass Moment of Inertia

For the ADCS, the S/C's mass moment of inertia has to be calculated. As mentioned in the centre of mass calculations, the propellant tanks and total S/C dry mass are the main component taken into account. Firstly, Equation 2.3 is used to compute the S/C's dry mass moment of inertia around the x-axis. This equation is derived from the equation illustrated in [8].

$$I_{\text{xx}} = m_{\text{dry}} \cdot r^2 \cdot \left(\frac{1}{3} + \frac{\sqrt{2}}{12} \right) \tag{2.3}$$

The propellant tanks are assumed to be a single spherical tank that holds the propellant mass. Using the volume of propellant tank $V_{\text{prop}} = 0.182\,69\,\text{m}^3$[3], the radius of the spherical tank is calculated to be 0.352 m.

The moment of inertia of this spherical tank along the x-axis can be computed using Equation 2.4 [9].

$$I_{\text{xx}} = \frac{2}{5} \cdot m_{\text{prop}} \cdot r_{\text{tank}}^2 \tag{2.4}$$

The inertia of the S/C dry mass in the shape of an octagonal prism and the propellant tank in the shape of a sphere is added together to acquire the total moment of inertia along the x-axis. Similarly the mass moment of inertia along the other axes can be obtained using the one of a cylinder around an axis perpendicular to its length[9]. Combining this with Equations (2.3) and (2.4) and taking into account that the propellant mass for station keeping decreases constantly over the mission, all mass moment of inertia equations are presented in Equation 2.5 and their values in Table 2.1.

$$\begin{aligned} I_{\text{xx}} &= m_{\text{dry}} \cdot r_{\text{cc}}^2 \cdot (1/3 + \sqrt{2}/12) + 2/5 \cdot m_{\text{prop,av}} \cdot r_{\text{tank}}^2 \\ I_{\text{yy}} &= 1/12 \cdot m_{\text{dry}} \cdot (3 \cdot r_{\text{cc}}^2 + h_{\text{S/C}}^2) + 2/5 \cdot m_{\text{prop,av}} \cdot r_{\text{tank}}^2 + m_{\text{prop,av}} \cdot d_x^2 \\ I_{\text{zz}} &= I_{\text{yy}} \end{aligned} \tag{2.5}$$

where

I_{xx} = mass moment of inertia around x-axis,
I_{yy} = mass moment of inertia around y-axis,
I_{zz} = mass moment of inertia around z-axis (see Table 2.1),
m_{dry} = dry mass of the S/C (1517.24 kg),
$m_{\text{prop,av}}$ = average propellant mass for station keeping (110.12 kg, from centre of mass),
d_x = the distance along the x-axis between the origin and propellant COM (0.702 m),
$h_{\text{S/C}}$ = height of the spacecraft (see Table 2.1).

Modes and time periods

There are two modes that need to be considered, mission and sending. During the mission mode, the S/C captures data, and has its x-axis pointing prograde and the y-axis in the nadir direction. During sending mode, the spacecraft sends data to Earth, and the x-axis points to Earth which is approximated in this report as aiming to the Sun and the spacecraft rotates around the y axis. Since no calculations have been made for the TT&C sub-system, an assumption is made that half of the time in sunlight the spacecraft sends data and the rest of the time it captures data.

The ranges are defined as follows: the ratio of the time in orbit before the S/C is in sunlight, is: $(0.5 - T_e/T_o)/2 = 0.0873$, where T_o is the point when the S/C x-axis is parallel to the solar rays. This results in the following ranges for each modes, sending: $[-0.0873 \cdot T_o, T_o/4]$ and mission: rest. The mission mode is subdivided in sunlight range: $[T_o/4, T_o/2 + 0.0873 \cdot T_o]$ and eclipse: $[T_o/2 + 0.0873 \cdot T_o, T_o - 0.0873 \cdot T_o]$. The orbital period, T_o, is 13 298.62 s.[3, tab. 2.5]

2.2. Environmental Disturbances on S/C

Environmental forces on the S/C create torques. These torques need to be countered by the ADCS system such that the S/C does not lose control. The main environmental forces that create disturbances are the aerodynamic drag, solar pressure, gravity gradient, and the magnetic field. As mentioned in Section 2.1, there are two modes that need to be considered, mission and sending.

Aerodynamic Drag Disturbance

Aerodynamic drag disturbance is caused by the drag experienced by the S/C while in orbit around Uranus. The factors which impact the aerodynamic torque are the design of the S/C and the orientation. The factors are taken into account in the vector r_d, the surface area S and the drag coefficient. C_D. Using Equation 2.7, the aerodynamic torque $\vec{\tau_d}$ is computed to be [0 Nm, 4.12×10^{-5} Nm, -4.12×10^{-5} Nm]. [6]

$$F_a = 0.5 \cdot C_d \cdot \rho \cdot v_o^2 \cdot S \tag{2.6}$$

$$\vec{\tau_d} = \vec{r_d} \times F_a \tag{2.7}$$

where

F_a = aerodynamic drag,
r_d = the vector from the S/C COM, C_m, to aerodynamic COP, C_p ([0.0649 m, 0.02 m, 0.02 m])[1],
C_d = drag coefficient (2.6)[3],
ρ = density at orbital altitude (8.417×10^{-13} kg/m^3)[3],
v_o = orbital velocity (13 988.86 m/s)[3],
S = surface area (see Section 2.1).

For the aerodynamic drag disturbances, the two modes are considered, mission and sending. For the mission mode, Equation 2.7 is directly used due to the velocity vector not changing with respect to the spacecraft axis system. For the sending mode, the torque is expressed as in Equation 2.8, using a fixed spacecraft axis system, with variable time, t. This is due to the change in pitch angle, θ, between the velocity vector and spacecraft axis system. The spacecraft must then leave its geodetic reference frame and point its x-axis to Earth. This is taken into account by giving the S/C a constant angular velocity, which is calculated using Equation 2.9. Thus, the angular velocity, ω, is 4.725×10^{-4} rad/s.

$$\vec{\tau_d} = \vec{r_d} \times 0.5 \cdot C_d \cdot \rho \cdot v_o^2 \cdot \begin{bmatrix} \sin^2(\omega t) S_x \\ \cos^2(\omega t) S_y \\ 0 \end{bmatrix} \tag{2.8}$$

$$\omega = \frac{2\pi}{T_o} \tag{2.9}$$

Using Equations (2.7) and (2.8), Figure 2.2 is generated. This figure illustrates the aerodynamic torque around each axis over the period of the orbit. As can be observed, there are instantaneous drops and rises in aerodynamic torque. This is because the spacecraft is assumed to be instantly back in mission mode after sending. However, in reality, the S/C would have to rotate back to its mission mode and vice versa.

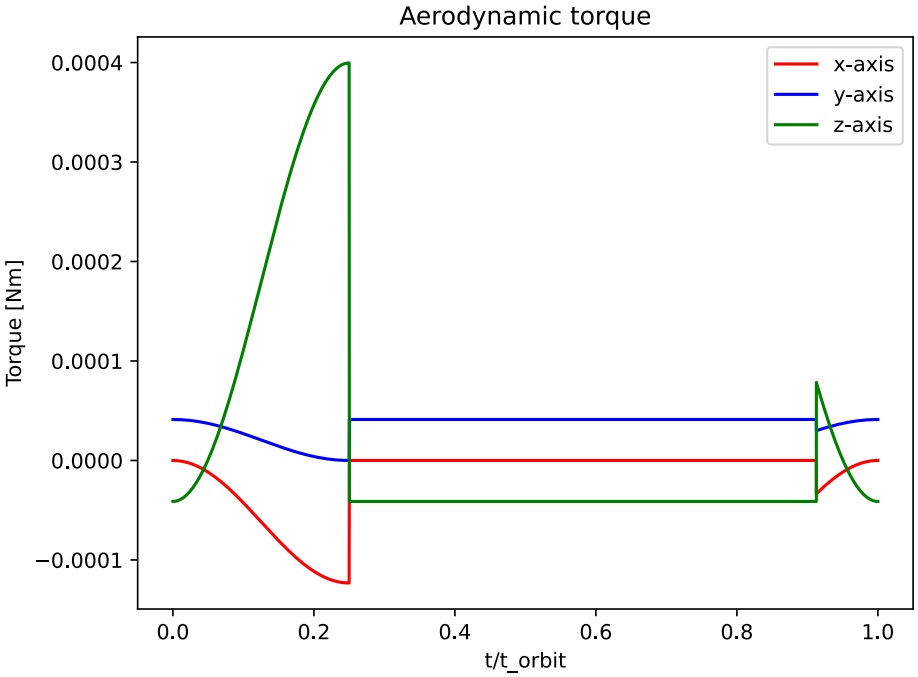

Figure 2.2: *Aerodynamic torque during orbit around each axis*

Solar Pressure Disturbance

Disturbance due to solar pressure is caused by solar radiation on the S/C. This generates a torque that has to be taken into account by the ADCS sub-system. Similarly to the aerodynamic torque, the solar radiation torque varies with the design and orientation of the S/C. The variables in this case are vector $\vec{r_s}$, the

[1] It is the distances of C_m assuming C_p is at the geometric centre

surface area S, and the reflectivity ρ. Using Equation 2.11, the solar torque $\vec{\tau_d}$ is computed to be [0 Nm, -3.79×10^{-8}Nm, 3.79×10^{-8}Nm].[6]

$$P_s = J_s / c \tag{2.10}$$

$$\vec{\tau_s} = \vec{r_s} \times ((1 + \rho_r) \cdot P_s \cdot S) \tag{2.11}$$

where

J_s = solar irradiance at Uranus (3.69 W/m^2)[5],
c = speed of light (~8×10^8 m/s),
$\vec{r_s}$ = vector from the S/C COM, C_m to the OCOP, C_o ([0.0649 m, 0.02 m, 0.02 m]) [2],
ρ_r = reflectivity of spacecraft (0.84)[3],
P_s = solar radiation pressure (1.234×10^{-8} Pa, computed using Equation 2.10),
S = surface area (see Section 2.1).

Similarly to the aerodynamic drag disturbances, the two modes are considered (mission and sending) only that mission mode only occurs when in sunlight. For the sending mode, Equation 2.11 is directly used due to the angle between the frontal surface and solar pressure staying constant. For the mission mode, the torque is expressed as in Equation 2.12, using a fixed spacecraft axis system, with variable time, t. This is due to the change in angle between the surfaces and the solar pressure.

$$\vec{\tau_s} = \vec{r_s} \times ((1 + \rho_r) \cdot P_s \cdot \begin{bmatrix} \sin(\omega t) S_x \\ \cos(\omega t) S_y \\ 0 \end{bmatrix} \tag{2.12}$$

Using Equations (2.11) and (2.12), Figure 2.3 is generated. This figure illustrates the solar torque around each axis over the period of the orbit. As can be observed, like the aerodynamic torque there are instantaneous drops and rises in solar pressure torque. This is because the spacecraft is assumed to be instantly back in mission mode after sending. However, the instant increase in solar torque at 91.27% of the orbital period is due to the S/C leaving eclipse.

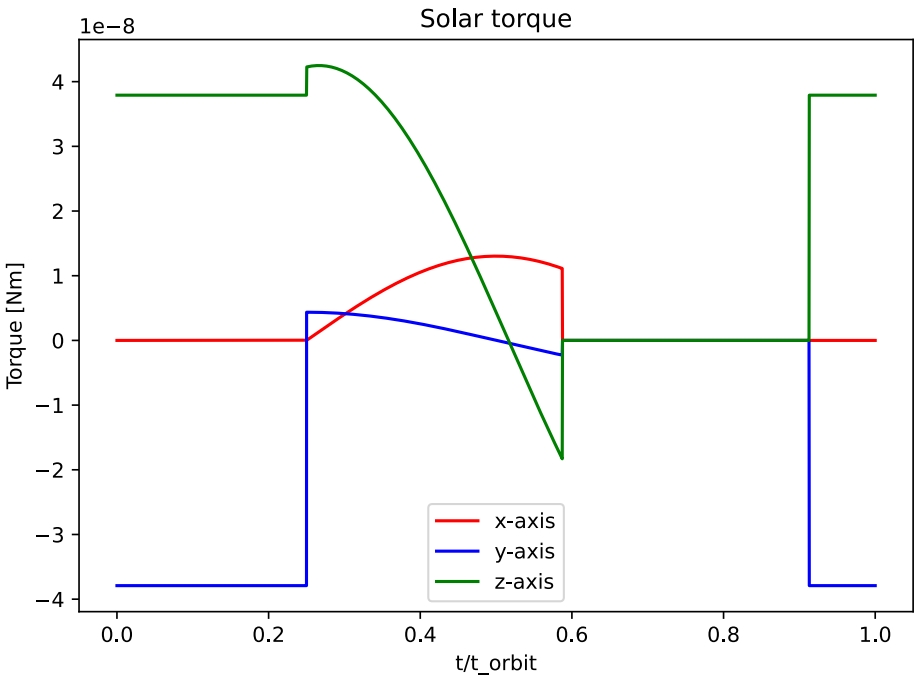

Figure 2.3: *Solar pressure torque during orbit around each axis*

[2]It is the distances of C_m assuming C_p is at the geometric centre

Gravity Gradient Disturbances

Gravity gradient torques are caused by a difference in the mass distribution of the S/C resulting in different mass moment of inertia along the three axis. Using Equation 2.13, the gravity torque is computed to be $[1.21 \times 10^{-6}\,\text{Nm}, 9.37 \times 10^{-5}\,\text{Nm}, 1.64 \times 10^{-6}\,\text{Nm}]$.[10, p. 115]

$$\vec{\tau_g} = 3/2 \cdot \Omega^2 \cdot \begin{bmatrix} (I_{zz} - I_{yy}) \cdot \sin 2\phi \cos^2\theta \\ (I_{zz} - I_{xx}) \cdot \cos\phi \sin 2\theta \\ (I_{xx} - I_{yy}) \cdot \sin\phi \sin^2\theta \end{bmatrix} \tag{2.13}$$

where

$\Omega = \sqrt{\mu / r_o^3}$ $(9491.99\,\text{s}^{-2})$[5],
I_{xx} = mass moment of inertia around x-axis,
I_{yy} = mass moment of inertia around y-axis,
I_{zz} = mass moment of inertia around z-axis (see Section 2.1),
ϕ = roll angle (1°),
θ = pitch angle (1°).[3]

Similarly to the aerodynamic drag disturbances, two modes are considered, mission and sending. For the mission mode, Equation 2.13 is directly used due to the angles not changing with respect to the spacecraft axis system. For the sending mode, the torque is expressed as in Equation 2.14, using a fixed spacecraft axis system, with variable time, t due to the change in pitch angle.

$$\vec{\tau_g} = 3/2 \cdot \Omega^2 \cdot \begin{bmatrix} (I_{zz} - I_{yy}) \cdot \sin 2\phi \cos^2(\omega t) \\ (I_{zz} - I_{xx}) \cdot \cos\phi \sin(2\omega t) \\ (I_{xx} - I_{yy}) \cdot \sin\phi \sin^2(\omega t) \end{bmatrix} \tag{2.14}$$

Using Equations (2.13) and (2.14), Figure 2.4 is generated. This figure illustrates the gravity gradient torque around each axis over the period of the orbit. As can be observed, like the aerodynamic torque and the solar pressure torque, there are instantaneous drops and rises in gravity gradient torque. This is because the spacecraft is assumed to be instantly back in mission mode after sending. However, in reality, the S/C would have to rotate back to its mission mode and vice versa. Additionally the torque around the x and z-axis are negligible compared to the one of the y-axis. This is due to the large difference in I_{xx} and I_{zz} and the magnitude of $\cos\phi$ and $\sin(2\omega t)$.

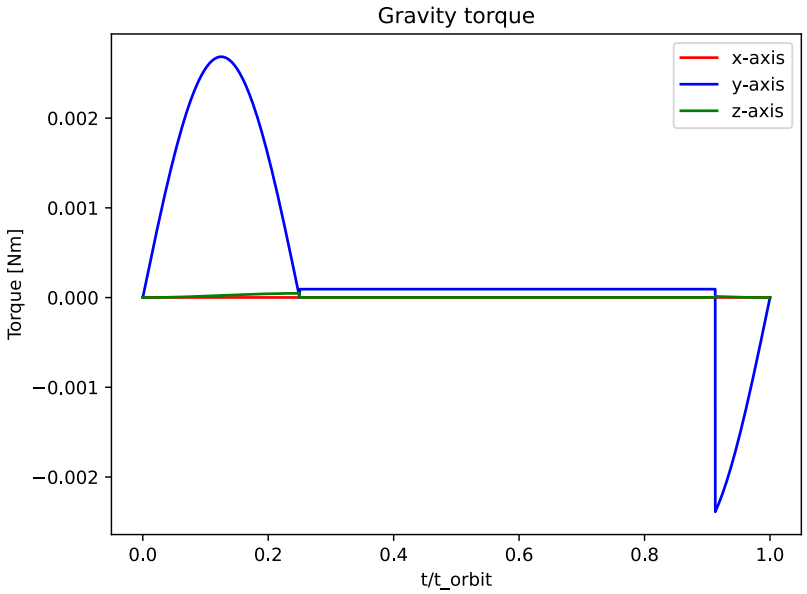

Figure 2.4: *Gravity gradient torque during orbit around each axis*

[3]This angle is assuming a misalignment of the S/C.

Magnetic Disturbance

Magnetic disturbances are caused by the effect of the magnetic field of Uranus on the S/C. Uranus' magnetic field is chaotic compared to Earth's, thus the ADCS has to be able to correct its attitude to successfully accomplish the mission[11, fig. 3]. No different modes are considered due to the torque being considered constant in orbit. Using Equations (2.15) and (2.16), the magnetic torque is computed to be 2.285×10^{-6} Nm.[7, p. 573]

$$B = \frac{M}{R^3}\lambda \tag{2.15}$$

$$\tau_m = D \cdot B \tag{2.16}$$

where

M = magnetic dipole moment Uranus (3.9×10^{17} Tm^3) [4],
R = distance between S/C and centre of Uranus (29 608 km) [5],
λ = unitless function of the magnetic latitude (1.2) [6],
B = magnetic field (2.285×10^{-5} T, computed using Equation 2.15),
D = residual magnetic dipole (0.1 Am^2)[6, p. 164].
τ_m = magnetic torque.

To acquire the magnetic torque over each axis, the magnetic declination and inclination with respect to the S/C are needed, but due to the complexity of the magnetic field of Uranus, these are difficult to acquire. Due to the complexity, at this moment in the design process, the magnetic torque is divided equally over each axis: $\tau_m/3$. Using this assumption, the magnetic torque array is computed to be [6.010×10^{-7}Nm, 6.010×10^{-7}Nm, 6.010×10^{-7}Nm]. This assumption does not decrease the final total impulse calculated in Section 2.4, nor the final propellant mass.

Using Equation 2.16, Figure 2.5 is generated. This figure illustrates the magnetic torque over the period of the orbit. Unlike the other graphs, this one does not illustrates the torque around each axis. This is due to the unknown magnetic torque around each axis.

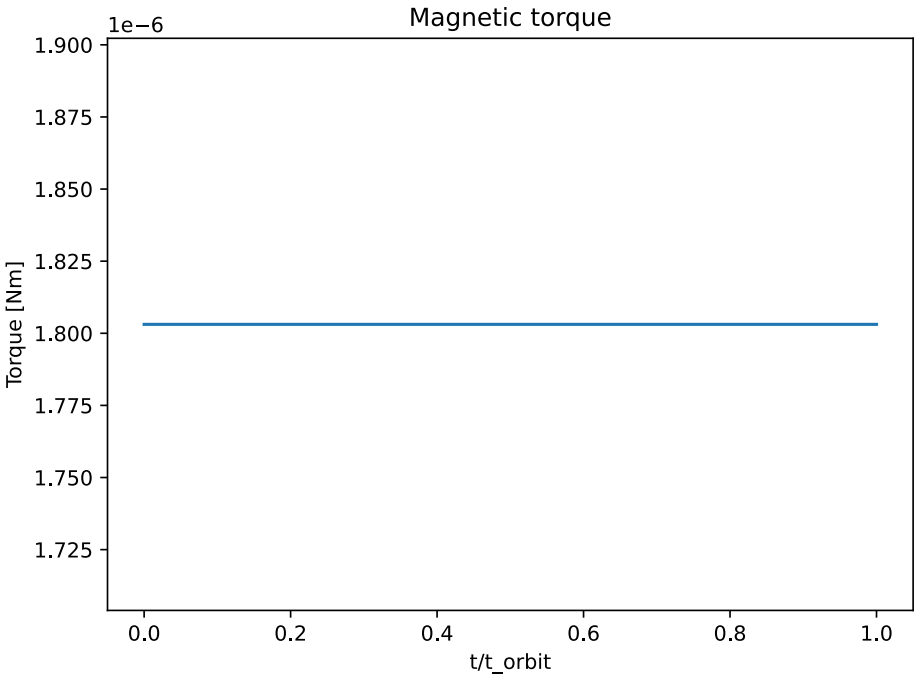

Figure 2.5: *Magnetic torque during orbit*

[4] It is 50 times larger than that one of Earth[7, p. 573][12, tab. 2.7]
[5] It is the sum of the average of the Uranus polar and equatorial radius,[5] and the orbital altitude[3]
[6] It ranges from 1 at magnetic equator to 2 at magnetic poles and is found using the 30° magnetic latitude of the mission orbit and [12, fig. 2.13b]

Total torque during orbit

The total torque on the spacecraft caused by the environmental disturbances is illustrated in Figure 2.6. This graph is composed by summing up the absolute value of each torque. This graph is similar to Figure 2.4 since the gravity torque is by a factor of 10 or more larger than the other torques.

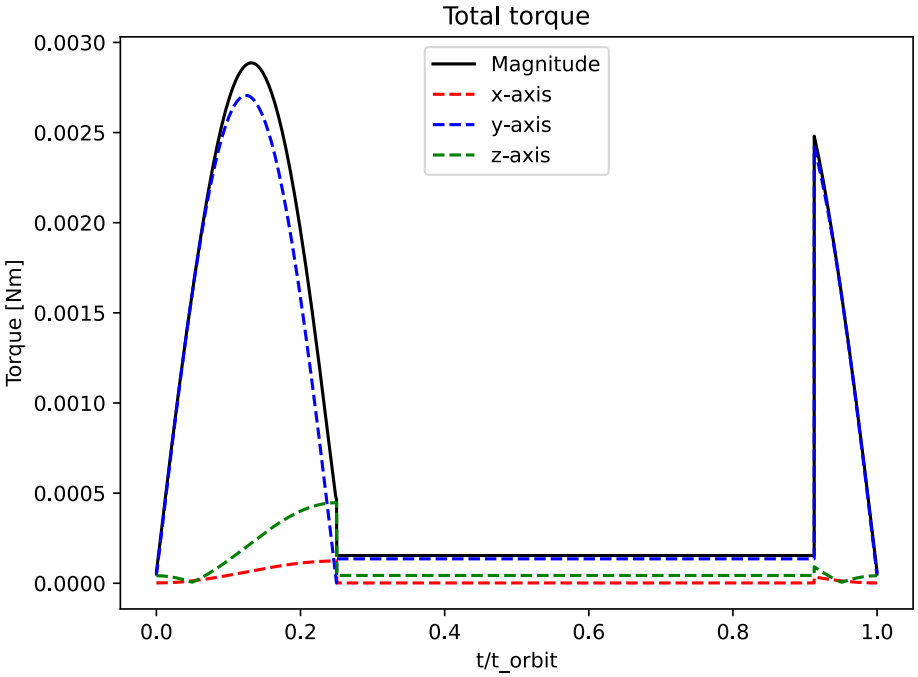

Figure 2.6: *Total torque during mission per axis*

2.3. Internal Disturbances of S/C

The internal disturbances within the S/C have various causes. These are often related to slight errors within the S/C which cause a torque. These can be caused by:

- a mismatch in thrust output between the ADCS thrusters (typical values of ±5%)[7, p. 574],
- a centre of gravity misalignment (typical values of 1 cm to 3 cm)[7, p. 574],
- main thruster misalignment (0.1 deg to 0.5 deg)[7, p. 574],
- vibrations caused by the momentum wheels[13],
- errors in communication between ADCS and TT&C [13],
- electrical and thermal interference due to the power, thermal and payload sub-system[13],
- and sloshing of the propellant[13].

The main disturbances are the misalignment of centre of gravity and the main thruster misalignment. The misalignment of the centre of gravity is already taken into account in the external disturbances, in Section 2.2. Thus the only one that still has to be taken into account is the disturbance cause by the main thruster misalignment. Additionally, to orient the S/C to Earth, it has to rotate. For this the S/C needs to change its momentum.

Disturbance Due to Main Thruster Misalignment

The position of the main thruster is assumed to be in front of the centre of mass with a misalignment angle of $\beta = 0.3°$ as suggested in [7, p. 574]. The misalignment can thus be calculated using Equation 2.17.

$$\vec{r_{\text{mt}}} = \begin{bmatrix} 0 \\ h_{\text{S/C}}/2 \cdot \sin\beta \\ h_{\text{S/C}}/2 \cdot \sin\beta \end{bmatrix} \tag{2.17}$$

Using the misalignment, the torque caused by the main thruster misalignment is calculated using Equation 2.18.

$$\vec{\tau_{\text{mt}}} = \vec{r_{\text{mt}}} \times F_{\text{T, mt}} \tag{2.18}$$

Assuming the centre of mass in the yz-plane is located in the geometric centre of that plane, the moment arm of the main thruster is $r_{\text{mt, y}} = r_{\text{mt, z}} = 0.0216\,\text{m}$, in y and z axes. The main thruster produce a thrust of 560 N which results in a disturbance torque of [0, 1.33 Nm, 1.33 Nm].

Rotation for sending

In order to send data to Earth, the S/C has to point its antenna to Earth. In order to do this, the S/C has to start rotating around the pitch axis with respect to the geodetic reference frame, as mentioned in Section 2.2. The change angular velocity to do this is 4.725×10^{-4} rad/s.

In order to obtain this angular velocity, the S/C has to change its angular momentum. The angular momentum L needed is calculated using Equation 2.19.[14]

$$L = I_{xx} \cdot \omega \tag{2.19}$$

2.4. ADCS Angular Impulse and Propellant Mass

To calculate the propellant mass for the ADCS, the angular impulse caused by the disturbances has to be calculated. In Subsection 2.4.1, the angular impulse will be calculated and presented, after which, in Subsection 2.4.2, the propellant mass needed will be calculated and presented.

2.4.1. Angular Impulse

Angular impulse is the change in angular momentum. It is calculated using Equation 2.20.[15]

$$\Delta L = \int \vec{\tau}\, dt \tag{2.20}$$

where

ΔL = angular impulse,
$\vec{\tau}$ = torque on the S/C,
dt = time increment.

As mentioned in Section 2.2, two modes during mission are considered: sending and mission mode. As mentioned in the power sub-system chapter in WP2, the S/C is 32.5% of its mission orbit in eclipse, T_e/T_o. This means that 67.5% of the orbit is in sunlight, T_d/T_o. With the assumption made that half of the time in sunlight the spacecraft is in sending mode, the spacecraft is 33.75% of mission orbit in that mode.

To calculate the impulses, the time periods have to be used. Using the time periods defined in Section 2.1, Equation 2.20, the torques in Sections 2.2 and 2.3 and the assumption, the angular impulse needed for the ADCS is calculated. The only torque that does not follow these periods is the main thruster misalignment torque. The dt for this torque is 1048.74 s or an average of 0.11 s per orbit.[7] In Table 2.2, all angular impulses per orbit are presented. The absolute integral is used by dividing the time in ranges. Since the ADCS thrusters do not have vector control, the total angular impulse per orbit is calculated by summing up all impulse, which results in a total of 18.189 Nms per orbit or 172 654.21 Nms for the entire mission

2.4.2. Propellant Mass & Volume

The propellant mass needs to be calculated to size the ADCS propellant tanks. Using Equation 2.23, the propellant mass is calculated. The propellant mass needed for each axis can be summed up because thruster pairs only burn around one axis. This equation is derived from Equations (2.21) and (2.22). Additionally, from these equations, the burn time equation, Equation 2.24, is derived.

$$\Delta L = F_T \cdot 2r_T \cdot t_b \tag{2.21}$$

$$F_T = \dot{m} \cdot I_{\text{sp}} \cdot g_0 \tag{2.22}$$

$$m_p = \frac{\Delta L_{\text{mis}}}{I_{\text{sp}} \cdot g_0 \cdot 2r_T} \tag{2.23}$$

[7] Assuming the mission time is 4 years, there are 9491.99 orbits

Table 2.2: *Angular impulse per orbit (in* Nms*)*

Disturbance\Mode	**Sending**	**Mission**
Aerodynamic	$\begin{bmatrix}0.218\\0.112\\0.596\end{bmatrix}$	$\begin{bmatrix}0\\0.363\\0.363\end{bmatrix}$
Solar	$\begin{bmatrix}0\\1.700\times10^{-4}\\1.700\times10^{-4}\end{bmatrix}$	$\begin{bmatrix}4.196\times10^{-5}\\1.058\times10^{-5}\\1.070\times10^{-4}\end{bmatrix}$
Gravity gradient	$\begin{bmatrix}5.684\\7.227\\8.304\times10^{-2}\end{bmatrix}$	$\begin{bmatrix}1.066\times10^{-2}\\0.826\\1.441\times10^{-2}\end{bmatrix}$
Magnetic	$\begin{bmatrix}7.993\times10^{-3}\\7.993\times10^{-3}\\7.993\times10^{-3}\end{bmatrix}$	
Main thruster misalignment	$\begin{bmatrix}0\\1.334\\1.334\end{bmatrix}$	
Total per orbit	$\begin{bmatrix}5.921\\9.870\\2.399\end{bmatrix}$	

$$t_b = \frac{\Delta L_o}{F_T \cdot 2r_T} \tag{2.24}$$

where

ΔL_{mis} = angular impulse for the mission (172 654.21 Nms, see Subsection 2.4.1),
ΔL_o = angular impulse per orbit (18.189 Nms, see Subsection 2.4.1),
F_T = thrust of ADCS thruster,
t_b = burn time of ADCS thrusters,
r_T = moment arm of the ADCS thrusters [4.12 m, 1.66 m, 1.66 m] [8],
$\dot{m}$ = mass flow of ADCS thruster,
I_{sp} = specific impulse of ADCS thruster,
g_0 = standard gravity of Earth (9.806 65 m/s^2).

The burn time is an array with the burn time for the thruster pair needed around each axis: [$t_{\text{b,x}}$, $t_{\text{b,y}}$, $t_{\text{b,z}}$].

Table 2.3 is a comparative table which includes propellant mass and burn time for different ADCS thrusters. The engines presented in this table are the engines with the highest specific impulse from Section 3.2. These engines produce the lowest propellant mass, based on the relation from Equation 2.23. As can be found in the table, the 5N-HPGP thruster at 5.5 N of thrust has the lowest burn time and propellant mass, however this comes at the cost of a higher power consumption. Since the thruster burn time is short, it is decided upon that the higher power consumption is not a limiting factor in this case and the 5N-HPGP thruster at 5.5 N will be the preferred choice for the ADCS. If the power would be limited during mission, the thrust could be lowered to 1.5 N and in such reduce the power consumption. This design choice will be further used in Section 3.2.

Thus, adding a 100% margin, the propellant mass needed for the ADCS is 35.69 kg. This margin comes from the Margin philosophy for science assessment studies of ESA.[16] Additionally, the burn time per orbit becomes [0.959 s, 3.956 s, 0.962 s].

To compute the total tank volume, Equation 2.25 is used. The density of the propellant, $\rho_{\text{prop, ADCS}}$ is 1240 kg/m^3 for LMP-103S (Table 3.10)[17, tab. 5]. This results in a propellant volume of 0.028 79 m^3 or 28.79 L.

$$V_{\text{p, ADCS}} = \rho_{\text{p, ADCS}} \cdot m_{\text{p, ADCS}} \tag{2.25}$$

[8] This is based on the geometry of the S/C, $[h_SC/2, s_proj/2, s_proj/2]$

2.5. Design Recommendations to Decrease Disturbances

The mass moment of inertia, centre of mass, and area are the major elements that can be optimised to increase the system's control effects on the S/C. The mass moment of inertia can be lowered by reducing the mass of the structures or the mass of the propellant required if all of the conditions are met with further iterations. The distance between the geometric centre of the octagonal prism and the S/C's centre of mass can be minimised by positioning the fuel tanks close to the S/C's centre of mass. Furthermore the surface area of the sub-systems outside the S/C can be lowered to reduce disturbances. Additionally, sensors and actuators that require less space and power are preferred.

Table 2.3: *Total mission propellant mass and burn time per orbit for the ADCS without margin*

Model	**Thrust**	**ISP**	**Power**	**Total mission propellant mass**	**Burn time per orbit**
[-]	[N]	[s]	[W]	[kg]	[s]
MR-111	4	229	16	18.62	$\begin{bmatrix}0.180\\0.742\\0.180\end{bmatrix}$
GR-1	1.1	231	12	18.47	$\begin{bmatrix}0.654\\2.697\\0.656\end{bmatrix}$
0.1N-HPGP	0.1	209	8	20.41	$\begin{bmatrix}7.189\\29.668\\7.211\end{bmatrix}$
5N-HPGP	1.5	239	15	17.85	$\begin{bmatrix}0.479\\1.978\\0.481\end{bmatrix}$
	5.5	253	25	16.86	$\begin{bmatrix}0.131\\0.539\\0.131\end{bmatrix}$

3

Sensors and Actuators for Attitude Determination and Control

In this chapter the different sensors and actuators for the S/C will be discussed (in Section 3.1 and Section 3.2 respectively), together with different technologies for each type and their characteristics. Sensors allow the S/C to calculate its orientation based on a reference system while actuators allow for the control of the attitude. After one particular model has been chosen for each type, possible configurations for both sensors and actuators will be mentioned in Section 3.3 along with their advantages and disadvantages, in order to later on choose one final configuration after performing a trade-off at the end of the chapter. All information on how these sensors and actuators work can be found in [14, 18], with the exception of the accelerometer, whose functioning can be found in [19].

3.1. Sensors

To be able to determine the S/C's attitude at all moments during the mission, sensors have to be used. Since the mission of the S/C is to the outer solar system and in a high orbit around Uranus, there are a few types of sensors that are not suitable.

First of all, magnetometers do not work at higher orbits. Therefore, they cannot be used on the UMO since it has an orbital altitude of 4343 km. Furthermore, in the case that the S/C would be in a low enough orbit, sufficient knowledge of the planet's electromagnetic field is required to use these. This does not apply to Uranus; thus, this type of sensor will not be considered.

For the Sun sensor, there are two types: a coarse Sun sensor, and a fine Sun sensor. Even though the coarse Sun sensor uses little to no power, the fine Sun sensor is more accurate and uses little power. It is therefore the one that will be considered for the S/C.

Additionally, a mechanical gyroscope would not be an appropriate choice, as moving parts reduce the lifetime of the components. This is not desirable for this mission with a duration of 20 years[2]. A preferred type of gyroscope would thus be a fibre optic gyroscope as it is a more advanced type of gyroscope and non-mechanical. This type will be considered for the S/C.

Lastly, an accelerometer will be considered along with the other sensors for the on-board computer to run more reliable simulations. The types of sensors that will thus be considered for the Uranus-Miranda orbiter are:

- Star sensors
- Fine Sun sensor
- Fibre optic gyroscope
- Accelerometers

The first two are absolute sensors (which measure the orientation of the S/C with respect to a reference plane) while the other two are relative sensors (which measures changes in the S/C's inertia). Both of these types will have to be present in the S/C to appropriately determine the S/C's attitude.

Star Sensors

Star sensors (STS) identify star patterns as seen from the S/C and compare them to the same patterns as seen from a reference system in order to determine the orientation and position. Each camera present in the S/C will provide one orientation vector out of the two needed to determine the S/C's absolute orientation. In order to ensure the S/C's orientation can be determined throughout the mission, there will be redundancy in the sub-system, meaning that 3 cameras will be present on the S/C, even if only 2 are working simultaneously.

Some models can be found in Table 3.1. Due to the higher accuracy and minimum mass and power, STAR-T3 will be considered for possible configurations.

Table 3.1: *Star Sensor's Data*

Name	**Mass**	**Power**	**Dimensions**	**Accuracy**	**Operating Temperatures**	**Update Rate**
[-]	[kg]	[W]	[mm × mm × mm]	[arcsec]	[K]	[Hz]
VST-68M [20]	0.47	3.0	60 × 60 × 138	5	253 – 338	5
VST-41M [20]	0.7 – 0.9	2.5	80 × 100 × 180	18	253 – 338	4
STAR-T3 [21]	0.35	2	60 × 60 × 88	2	233 – 323	5

Sun sensors

Sun sensors (SNS) determine the direction of the Sun-rays relative to the S/C. This sensor provides one vector to compare to the reference system, as there is only one Sun present in our Solar system. There exist to types of Sun sensors, coarse Sun sensors and fine Sun sensors. Fine Sun sensors can deliver higher accuracy than coarse Sun sensors, although they usually require more power . Different models of Sun sensors can be found in Table 3.2. Due to the higher accuracy and minimal mass, the S3 model will be the one considered for the different configurations.

Table 3.2: *Different models of Sun sensors*

Name	**Mass**	**Power**	**Dimensions**	**Accuracy**	**Operational Temperature**
[-]	[kg]	[W]	[mm × mm × mm]	[arcsec]	[K]
S3 [22]	0.33	0.7	112 × 112 × 43	72	248 – 333
Mini Fine Sun Sensor [23]	0.05	0	50 × 46 × 17	720	223 – 353
Fine Sun Sensor [24]	0.375	0.25	108 × 108 × 52.5	1080	223 – 358

Fibre Optic Gyroscope

A fibre optic gyroscope (FOG) works by splitting a laser beam into two and then entering different fibre coils which rotate in opposite directions. The different paths of these beams cause different travel times due to the Sagnac effect and are measured by a detector. By rotating, the S/C modifies the phase difference. This difference is measured by the detector and compared to the original travel-time difference to calculate the S/C's new relative attitude. Different models of laser gyroscopes can be found in Table 3.3. Note that the first dimension on the "Dimensions" column refers to diameter and the second one to height. Due to the minimum mass and size, the GS-FOG50A will be the one considered for the different configurations.

Table 3.3: *Fibre Optic Gyroscope Models*

Name	**Mass**	**Power**	**Dimensions**	**Operating Temperatures**
[-]	[kg]	[W]	[⌀mm × mm]	[K]
GS-FOG50A [25]	0.160	3	50 × 33.5	233 – 333
GS-FOG60A [26]	0.160	3	60 × 34.7	233 – 338
GS-FOG70A [27]	0.285	3	70 × 32	233 – 333

Accelerometer

An accelerometer (ACC) is a device that measures non-gravitational acceleration of a body along three axis by generating a current proportional to the force applied on it. Since the mass of the device is constant, Newton's second Law is then used to determine the acceleration of the body along that axis [19]. Different models of accelerometers can be found in Table 3.4. Note that the sensitivity refers to the minimum voltage detected per unit mass of the sensor; a lower sensitivity results in a more accurate sensor. For this reason, and since it measures acceleration on all three axis, the 3313A1 model will be used.

Table 3.4: *Accelerometer Models*

Name	**Mass**	**Power**	**Dimensions**	**Sensitivity**	**Operating Temperatures**
[-]	[g]	[W]	[mm × mm]	[V/kg]	[K]
3313A1 [28]	4.1	0.6	9.1 × 11.9 × 17.7	1	222 – 394
331A43H [28]	4.1	0.6	9.1 × 11.9 × 17.7	10	222 – 436
GS-JBK-9 [29]	100	0.48	30 × 30 × 32	1.7	218 – 368

Possible Sensor Configurations

In order for the ADCS sub-system to be fully redundant and provide no points of failure at eclipse and full sunlight, at least three star sensors will be present in the S/C, out of which only two will operate simultaneously. Furthermore, Sun sensors will be included since it will provide a position vector, allowing one of the star sensors to stay on stand-by, thus saving power.

Additionally, at least four gyroscopes and two accelerometers will have to be present in the S/C in order to provide accurate measurements of the linear and angular parameters of the S/C with full redundancy and no single points of failure. The possible configurations and their properties can thus be found in Table 3.5.

Table 3.5: *Possible configurations of sensors for the ADCS*

Configuration	**Amount**				**Total Mass**	**Average power**	**Average accuracy**
[-]	SNS	STS	FOG	ACC	[kg]	[W]	[arcsec]
1	0	3	4	2	2.07	15.6	5.0
2	1	3	4	2	2.40	14.0	50.2
3	2	3	4	2	2.73	14.0	50.2
4	3	3	4	2	3.06	14.0	50.2

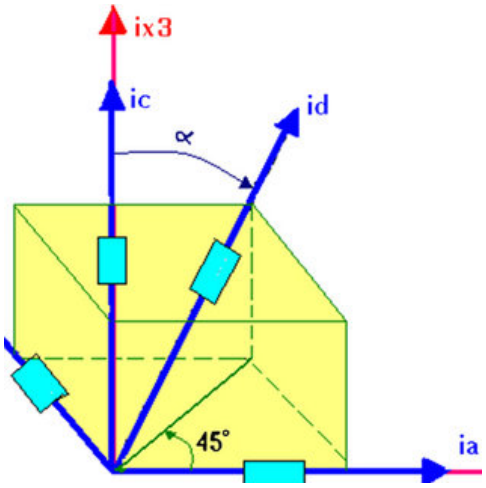

Figure 3.1: *Gyroscope Configuration (retrieved from [30])*

In all configurations, three of the FOG will be perpendicular to each other and the fourth one will be at an angle of 45° with the rest, as illustrated in Figure 3.1 and the star sensors will all be perpendicular to each other. Note that the average power and accuracy presented in Table 3.5 were calculated under the assumption that the Sun sensors will work during the entire time the S/C is not in eclipse (thus 67.4% of the orbit [3]). If higher accuracy is required, another star sensor could be turned on, increasing the accuracy up to 5 arcsec.

Regarding the Sun sensor, one will be placed next to the antenna. It will be pointed at Earth which is be close enough to the Sun with respect to the distance of Uranus. In the third configuration, the second Sun sensor will be placed next to the original one; and lastly, in the fourth configuration, one Sun sensor will be placed next to the antenna, and the other two will be placed on the sides of the S/C opposite of each other.

The first configuration minimises mass, which is advantageous. However, the power consumed will always be the maximum value. The second configuration, is more massive than the first one, however reduces power consumption during majority of the mission orbit (the time it is not in eclipse). However, if the Sun

sensor fails, mass will have been added to the S/C as compared to the first configuration and the power consumed would still be the same; problem that is solved in the third configuration. Lastly, the main advantage of the fourth configuration is that it minimises power consumption independently of the S/C's orientation, which could be beneficial during transfer, where power consumption is critical in order to cool down the S/C, as stated in WP2.[3]

3.2. Attitude Control Actuators

Attitude control plays a vital role throughout the operating life time of the S/C. It paves the way for accurate and stable payload measurements, antenna pointing as well as orbital manoeuvres. There are two main approaches to attitude control, namely passive and active control.

Passive attitude control is characterised by a lack of actuators. Control is obtained by cleverly designing the S/C to make use of surrounding fields or its rotation[6]. This category can be divided in to four different methods.

The first one is pure stabilisation spin around one axis. This method relies on the gyroscopic stiffness induced on the perpendicular axis with respect to the rotation axis. For the UMO, this strategy is not applicable because the payload requires the S/C to not rotate. A similar option is the the dual spin stabilisation. This approach makes use of the same gyroscopic stiffness as the previous method while keeping the payload from rotating. However, this solution requires a complex structure associated with higher mass and lower reliability. Furthermore, the estimation found in [3] explains that the ADCS sub-system requirements are achievable by less involved methods.

Another method is to rely on external fields such as the gravitational and magnetic field in the vicinity of Uranus, however, these methods are unfeasible for the UMO. The gravity gradient approach requires the S/C to have an extended mass distribution along the nadir direction. However, the UMO has a mass distribution extending tangent to the orbit. This creates an undesired gravity gradient which will has been taken into account during the calculation of the disturbance torques. Furthermore, the chaotic magnetic field of Uranus renders impossible any attempts to use magnets or hysteresis rods to control the attitude. Hence, one has to consider active stabilisation.[11]

Active attitude control relies on controlling the attitude of the S/C with actuators. These create torques of two different types: internal and external.

Internal torques are generated by changing the angular velocity of rapidly spinning wheels. Courtesy of the conservation of angular momentum the rotations around the axis can be manipulated. The three main types of wheels are reaction wheels, momentum wheels and control moment gyros. External torques will treated in separate section later in the report.

Momentum and Reaction Wheels

Reaction wheels are stationary in their nominal configuration and start turning to counteract disturbance torques. To achieve three axis stabilisation, at least three reaction wheels placed perpendicular to each other are needed. This is the simplest approach to attitude control which provides the highest reliability due to its mechanical simplicity. They are often used in smaller form factor S/C. Similarly to reaction wheels, momentum wheels counteract disturbances torques by changing their angular speed. The difference between momentum wheels and reaction wheels lies in the nominal velocity which is non-zero in momentum wheels. This allows them to provide gyroscopic stiffness along the axis perpendicular to the rotation axis, however, due to the constant moving parts, momentum wheels tend to have lower lifetime and higher failure rates. Because of the similarity in operational principles, reaction wheels can be often used as momentum wheels. In Table 3.6 a comparison of reaction and momentum wheels is presented for prime understanding of the overall performance of the technology.

Control moment gyro

Control moment gyro (CMG) is the next actuator of interest. This component is built up of a reaction wheel and gimbals, which allows the reaction wheel to rotate around a pivot. Torque can be created by changing the spinning axis of the wheel. This method tends to deliver higher temporary torques and larger power efficiency compared to reaction wheels due to the lack of acceleration or deceleration within the mechanism. This technology is applied more frequently for larger S/C, due to its more complex, larger and heavier form

Table 3.6: *Comparison of reaction and momentum wheels*

Actuator model	**Momentum storage**	**Torque**	**Mass**	**Size**	**Power**	**Lifetime**
[-]	[Nms]	[Nm]	[kg]	[⌀mm × mm]	[W]	[yr]
HR16 [31]	50 75, 100	0.1–0.4	9, 10.4, 12	418 × 178	22–105, 195	15
RWA-15 [32]	20	0.68	14	369 × 153	230	7
VRW-D-4 [33]	4	0.5	2.5	180 × 60	65	5
RC4-17.0 [34]	17	0.3	24.4	497 × 265	141	-
RW1000 [35]	15	1	11.5	337 × 121	10–160	8

factor. When designing for ADCS two CMG are required for full redundancy. In Table 3.7 a comparison of control moment gyros is presented.

Table 3.7: *Comparison of different control moment gyros actuators*

Actuator model	**Momentum**	**Torque**	**Mass**	**Size**	**Pointing performance**	**Power**	**Lifetime**
[-]	[Nms]	[Nm]	[kg]	[mm × mm × mm]	[mrad]	[W]	[yr]
CMG 15-45 S	15	45	18.4	mechanism: ⌀270 × 350, electronics: 310 × 300 × 150	<10	25	10
CMG 40-60 S	30-40	60	38	mechanism: 370 × 465 × 500, electronics: 310 × 210 × 175	<1	55	10
CMG 75-75 S	70-75	75	69	mechanism: 550 × 500 × 570, electronics: 390 × 250 × 175	<0.1	37-160	10
CMG-12	12	12	15	340 × 43 × 380	-	20-35	10
M50	25-75	75	28	mechanism: ⌀714 × 131, electronics: 264 × 238 × 102	-	11-113	-

Trade-off data comparing the considered actuator technologies is found in Table 3.8. The trade-off criteria and the according weights are based on requirements provided in WP2 [3] and overall mission needs. Every technology is rated on a scale from zero to ten, where ten represents the optimal performance and zero represents the lowest possible performance, of a given technology in certain field. All values are chosen based on engineering judgement, meaning they do not have any official meaning or foundation. The presented trade-off will not be used to choose one particular actuator technology, but it will be considered in Section 3.3 when creating the design options. It is clear that the CMG exceeds or matches all other technologies in performance in every criterion, making it the optimal option for the UMO S/C.

Table 3.8: *Trade-off table of the different actuators technologies*

-	Tradeoff criteria							-
-	**Total momentum storage**	**Torque**	**Mass**	**Gyroscopic stiffness**	**Cost**	**Reliability**	**Power**	**Total**
Actuator technology\Weight	30%	15%	20%	10%	5%	10%	10%	100%
Reaction Wheel (RW)	6	3	4	3	3	7	5	4.7
Momentum wheel (MW)	6	4	4	9	3	6	5	5.35
Control moment gyro (CMG)	8	9	8	9	4	6	5	7.55

Thrusters and external torques

External torques are created by applying the principle of action-reaction. Two systems are widely used within the space industry to generated external torques. More commonly, thrusters are used to generate torques. By arranging the thrusters parallel to each other and firing them at the same time a moment couple is produced around an axis perpendicular to the lever arm between the thrusters. By disposing multiple pairs of these thrusters on the S/C surface, complete three axis control can be achieved. The other possible solution is to use magnetic torquers to generate torques around the desired axis. However, in the context of Uranus' chaotic magnetic field [11], this solution is not viable. The only solution to create external torques is to use control thrusters to correct the attitude. Several different thruster technologies are compiled and presented in Table 3.9. Values used for the trade-off criteria are evaluated based on the detailed analysis found in [36].

Table 3.9: *Trade-off table of the different thruster technologies*

-	Tradeoff criteria							-
-	**Mass**	**Size**	**Thrust**	**Power**	**Reliability**	**Efficiency**	**Safety**	**Total**
Actuator technology\Weight	10%	10%	20%	20%	20%	10%	10%	100%
Hydrazine Mono-propellant	7	7	8	8	9	4	2	7
Other Mono/Bi-propellant	5	5	8	8	7	6	6	6.8
Hybrids	3	3	7	6	5	3	8	5.3
Cold/Warm Gas	6	6	4	6	8	4	8	6
Solid	4	4	9	6	8	3	3	6
Electrothermal	5	5	8	3	8	7	7	6.2
Electrospray	6	6	5	3	6	9	4	5.3
Gridded Ion	4	4	5	3	4	8	6	4.6
Hall Effect	6	6	6	3	8	9	7	6.2

Based on the results presented in chemical propulsion thrusters are advantageous, compared to other options. Of those, hydrazine and other mono/bi-propellants are the optimal options for UMO S/C. Hydrazine is frequently used propellant for deep space probes because it is a highly reliable and proven propellant.[36] This provides the designer with a wide variety of components available on the market. The downside of using hydrazine is the significant environmental footprint. Hydrazine is "corrosive, toxic and potentially carcinogenic" as described in [36]. This results in a trend to shift towards new and more environment-friendly propellants. However, these newer technologies are not as mature and flight proven which can be risky for a mission to Uranus. In consequence both options will be considered for the design of the UMO. An overview of several thrusters is illustrated in Table 3.10.

Table 3.10: *Comparison between different chemical thrusters*

Model	**Propellant**	**Thrust**	**ISP**	**Mass**	**Power**	**Status**
[-]	[-]	[N]	[s]	[kg]	[W]	[-]
MR-111 [37]	Hydrazine	4	219–229	0.37	16	F
AG - 1N [38]	Hydrazine	0.3–1.1	200–223	0.29	N/A	F
Monarc-5 [39]	Hydrazine	4.5	226	0.49	18	F
GR-1 [40]	AF-M315E	0.4–1.1	231	N/A	12	F
0.1N-HPGP [41]	LMP-103S	0.03–0.1	196–209	0.38	6.3-8	E
5N-HPGP [41]	LMP-103S	1.5–5.5	239–253	0.48	15-25	D
BGT-X1 [42]	AF-M315E	0.02–0.18	214	N/A	4.5	D
BGT-5 [42]	AF-M315E	1–6	230	N/A	50	D

Table 3.10 presents a variety of different types of actuators to be considered. Depending on the desired configuration that the designer can choose between different levels of thrust. The F grade in the reliability indicates that the actuators is flight proven across multiple mission and demonstrated consistent performance. The D grade depicts that the actuators is still in development while grade E denotes that the actuator is schedules to be tested on a mission. Specific thruster models used by UMO will be determined after complete ADCS configuration is finalized.[36]

Possible Actuator Configurations

In order for the actuator configuration to be feasible for the UMO ADCS, a number of factors must be taken into account. First of all, the system needs to be fully redundant, meaning that no single points of failure can be present in the configuration. Additionally, when considering reaction wheels, momentum wheels or control moment gyros, the problem of saturation has to be considered. This can be solved by means of external torques with use of thrusters to desaturate the S/C. Possible actuator configurations are presented in Table 3.11.

Table 3.11: *Possible configurations of actuators for the ADCS*

Configuration	Amount				Total momentum storage	Total torque	Power	Total mass
-	RW	MW	CMG	Thruster	[Nms]	[Nm]	[W]	[kg]
1	0	0	2	12	24	24.0	220 – 370	35.7
2	4	0	0	16	60	4.0	280 – 1040	53.7
3	0	0	0	16	-	1.4	170 – 264	6.9
4	0	4	0	8	200	0.4	208 – 980	39.8

For configuration number one, two CMG-12 CMG's and twelve 5N-HPGP thrusters are considered. This configuration type is often used in larger S/C, due to the high torques it can achieve. The system is fully redundant, although a problem that needs to be considered is the potential appearance of a phenomena known as singularities, which needs to be avoided by means of a software. The CMG's are designed to avoid anti-parallel alignment, which will cause loss of control around one of the axis. The thrusters are mainly responsible for dumping excess momentum in case of a CMG's saturation, but can be used for other manoeuvres. The CMG's technology allows for low power consumption when in use.

The second configuration uses four RW1000 RW's and sixteen 5N-HPGP thrusters. Compared to the previous configuration, RW's instead of CMG's are used. Four RW's are required, one for each axis and one to ensure full system redundancy. Thrusters are still required for momentum dumping. The split into multiple reaction wheels solves the problem with singularities and anti-parallel alignment, which makes this option less likely to fail during the entire mission duration. Unfortunately, using reaction wheels requires more power than CMG when performing similar tasks and deliver less torque on average. The fourth RW is mounted in a slewed position, this provides control around all three axes of the S/C, even in the case of a RW failure.

For configuration number three, only thrusters are considered for control. It contains eight 5N-HPGP and eight 0.1N-HPGP thrusters. This configurations does not containt any moving parts which it makes more reliable. Furthermore the substantial advantage of this configuration is the low mass, due to lack of any RW's or CMG's. This advantage is partly counteracted with increase in propellant mass and number of propellant tanks. Another disadvantage is the lower slew rate due to a lower maximum torque.

The fourth and last option taken for consideration requires four HR16 momentum wheels together with eight 5N-HPGP thrusters, which ensures the ADCS sub-system fully redundant. The momentum wheels still needs to be desaturated by means of the thrusters, but due to the fixed positioning of the wheels there is no concern with anti-parallel alignment and singularities. Similarly to CMG's, momentum wheels have gyroscopic stiffness and require less power to operate. Unfortunately the momentum wheels will deliver torques values similar to RW's values, which are considerably smaller when compared to CMG's.

3.3. Attitude Determination and Control Sub-system Configurations

Design option generation is an important step of every design process. Creating multiple configurations provides an opportunity to compare and evaluate possible design choices. In this section all possible sensor and actuator configurations for the ADCS sub-system of the Uranus-Miranda orbiter will be presented and evaluated by means of a trade-off table. In Section 3.1 and Section 3.2 the separate configurations for the sensors and actuators have been formulated. Now, they can be combined in multiple ways to create several possible ADCS sub-system options.

Design Option Generation

Four possible design options were decided upon for the UMO ADCS. This number allows for the emergence of a variety of different configurations while keeping the number sufficiently small to allow for individual

exploration. The aim of these designs was to investigate the impact of different type of technologies and ADCS configurations on the S/C architecture.This allows for better overview of possible design options, consequently following with better final design. It is important to note that the Figure 3.2 to Figure 3.5 are not to scale. Their aim is to provide visual support to the text.

The first option, displayed in Figure 3.2, combines sensor configuration number two and actuator setup number one, meaning it uses one Sun sensor, three star sensors, four fibre optic gyroscopes and two accelerometers for taking ADCS measurements and two control moment gyros, together with twelve thrusters for control. This option is an appropriate combination of performance with feasible power and mass budget. Having two CMG's, combined with twelve thrusters for desaturation provide the S/C full range manoeuvrability and redundancy. The 12 thrusters allow for optimal rotational control which means that the S/C can rotate alongs its axis without any translation. The actuator model chosen are the CMG-12 gyroscopes and the 5N-HPGP thrusters. The thrusters will be powered by two propellant tanks located in the middle of the S/C. Furthermore, the star sensors will provide a high accuracy of the S/C's orientation and position, while saving power during down-link where it might be needed by the TT&C sub-system.

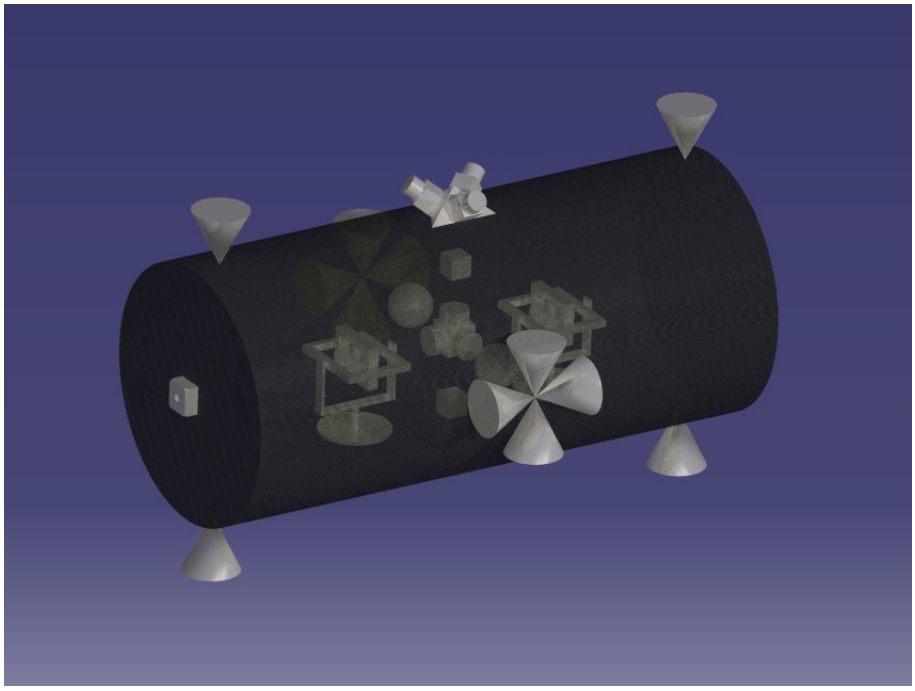

Figure 3.2: *Option 1 of the Uranus-Miranda orbiter*

Option number two uses the sensor configuration number one and actuator configuration number three, it is illustrated in Figure 3.3. It uses three star sensors, four fibre optic gyroscopes and two accelerometers for taking ADCS measurements and not less then sixteen thrusters for control. Those are divided into two thrust categories. The smaller thrusters provide the S/C with precision attitude control needed to counteract the disturbances while the larger thrusters are used for rotating the S/C during transmission or other maneuvers. This configuration comes with two propellant tanks of different sizes for each group of thrusters. This option is the mass and power budget optimal configuration. The high sensor accuracy together with eight 0.1N-HPGP low-thrust thrusters makes the system more accurate, when comparing it to the other options. Another eight 5N-HPGP thrusters are used for higher disturbance torques.

The third option combines the sensor configuration number three and actuator configuration number two giving the design illustrated in Figure 3.4. It uses two Sun sensors, three star sensors, four fibre optic gyroscopes and two accelerometers paired with four reaction wheels and sixteen thrusters for control. This configuration is presented with 3 propellant tanks. The additional thrusters combined a fully redundant 4 RW setup in a pyramid configuration, together with two Sun sensors (in case of failure of one of them) makes this option reliable and provides optimal control and high precision. Unfortunately, the amount of high power ADCS components has an impact on the power and mass budget.

The last design option includes the fourth configurations for both sensors and actuators. A visual representation of it is illustrated in Figure 3.5. The fourth actuator configuration, which includes four momentum

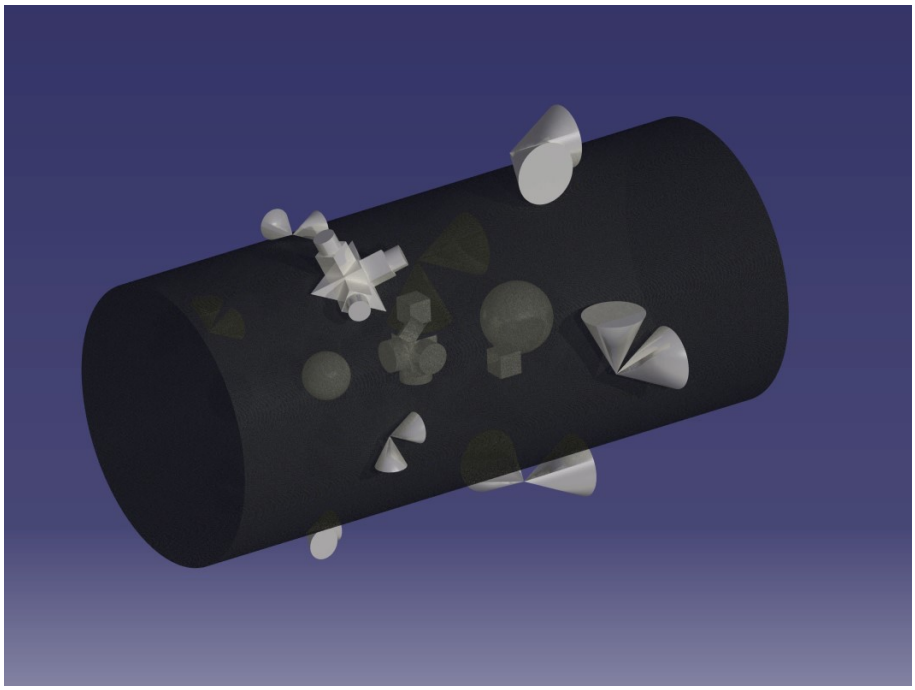

Figure 3.3: *Option 2 of the Uranus-Miranda orbiter*

wheels and eight 5N-HPGP thrusters, has a relatively high power budget and it is not compensated as in option three in terms of performance. The eight thruster configuration does not allow for pure rotation along all the three axis. If one of the thrusters fails, only seven thruster remain for desaturation which can cause complication in later mission phases. However the clever alignment allows for three axis control while limiting the spread of thruster around the S/C minizing the propellant tubing. Moreover, it uses RW1000 as momentum wheels, mounted in a pyramid configuration to provide redundancy.

An overview of all described options is presented in Table 3.12.

Table 3.12: *Possible options for the ADCS sub-system*

Parameters\ Options	**Unit**	**Option 1**	**Option 2**	**Option 3**	**Option 4**
Sensor config. number	-	2	1	3	4
Sensor config.	-	1 SNS, 3 STS, 4 FOG, 2 ACC	0 SNS, 3 STS, 4 FOG, 2 ACC	2 SNS, 3 STS, 4 FOG, 2 ACC	3 SNS, 3 STS, 4 FOG, 2 ACC
Actuator config. number	-	1	3	2	4
Sensor config.	-	2 CMG, 12 thrusters	16 Thrusters	4 RW, 16 thrusters	4 MW, 8 thrusters
Total mass	[kg]	38.1	9.0	56.4	42.9
Power range	[W]	234.0 – 384.0	185.6 – 279.6	294.0 – 1054.0	222.0 – 994.0
Sensor accuracy	[arcsec]	50.2	5.0	50.2	50.2
Total torque	[Nm]	24.0	1.4	4.0	0.4
Total momentum storage	[Nms]	24.0	-	60.0	200.0

Trade-off

To perform a valid trade-off analysis a choice of trade-off criteria together with corresponding weights is determined. This step has been discussed and agreed upon between the members of the ADCS design team, based on the requirements presented in WP2 [3] for the ADCS sub-system and the overall needs of the mission

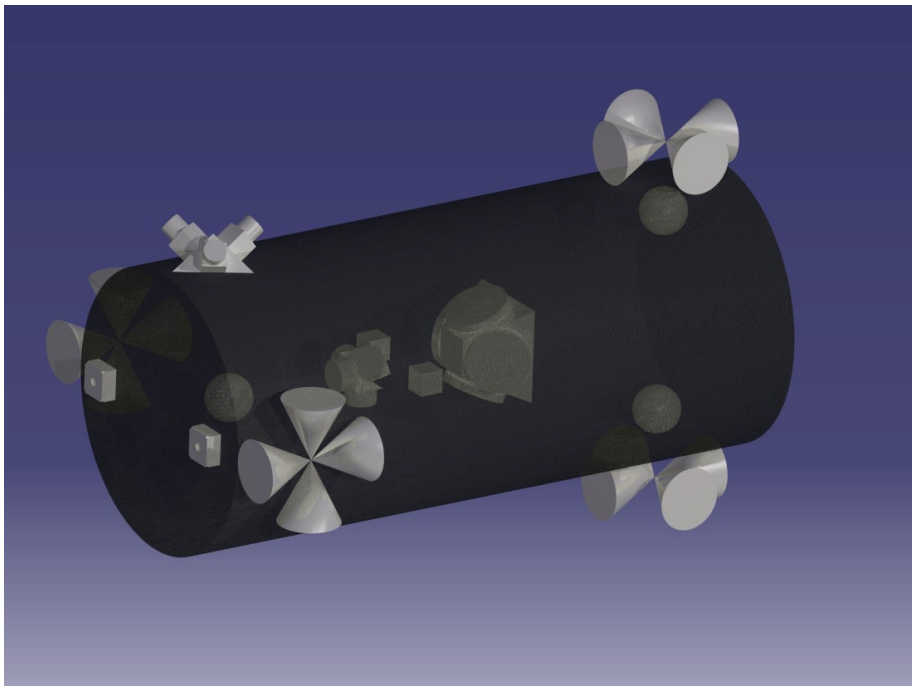

Figure 3.4: *Option 3 of the Uranus-Miranda orbiter*

profile. The results are presented in Table 3.13.
Power and mass are the crucial factors when designing the sub-system, since they are both the main constraining parameters in the mission design. Mass needs to be minimised to make it possible for the launcher to deliver the S/C to the desired orbit. Power needs to be constrained to fit the power budget, otherwise more electrical power will be used than produced by the power sub-system, causing unwanted shutdowns and failures of other sub-systems. Both of these criteria were assigned with weight of 30 % with together makes over half of the total. Other criteria like torque produced, accuracy or reliability have been rated 20%, 10%, 10% respectively. Those values are lower in comparison to mass and power, because they are not considered as important and are seen as functional, rather than constraining criteria if the main requirements are met.

The next step in deciding upon the final design of the UMO ADCS sub-system is evaluating the design options against the trade-off criteria. This can be done by means of a trade-off table, presented in Table 3.13. It is important to note that the input relies mostly on engineering judgement, thus all values do not have any official meaning or scientific foundation. The criteria are evaluated for every option on a scale from one to ten, similarly to previous trade-off tables presented in section Section 3.2.

Table 3.13: *Trade-off table of the different ADCS sub-system options*

-	Trade-off criteria					-
-	**Mass**	**Power**	**Performance**	**Accuracy**	**Reliability**	**Total**
Option/Weight	30%	30%	20%	10%	10%	100%
Option 1	6	7	9	6	8	7.1
Option 2	9	8	3	8	4	6.9
Option 3	3	3	5	6	8	4.2
Option 4	5	4	2	6	6	4.3

When evaluating the options against the trade-off criteria some configurations can be more favourable than others in different aspects. Option two is the leading option in terms of mass. Since it is using only smaller thrusters for ADCS, weight is significantly decreased due to lack of any RW's. When looking at the power criterion, option two is still considered the leading configuration. It has a power advantage compared to the other options, although option number one has more advantageous values than options three and four. Option two has clearly dominated in terms of power and mass, but in order to do that a compromise had to be done in terms of performance. When evaluating the options in terms of the performance criterion,

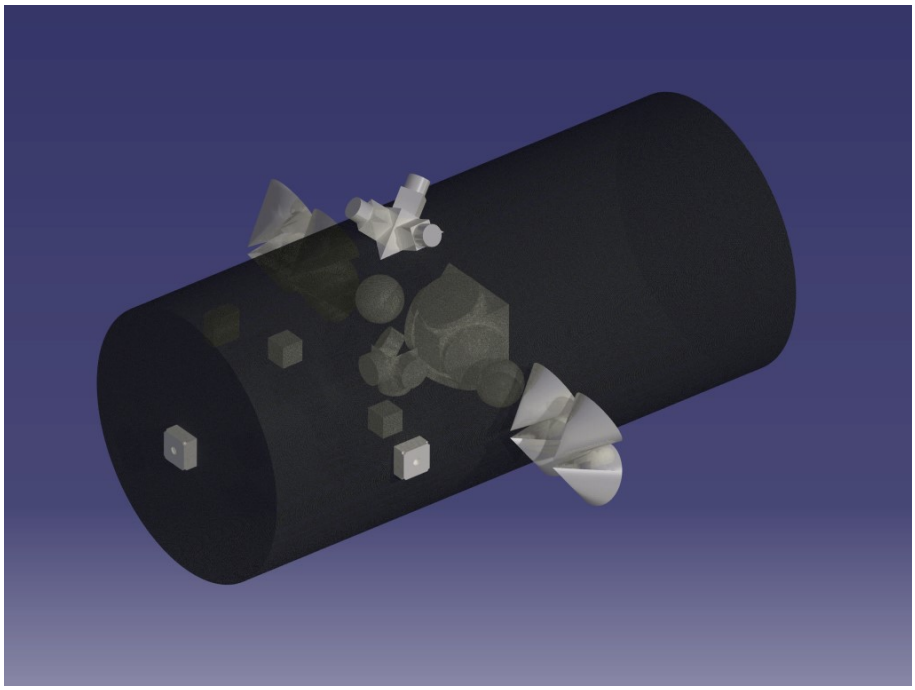

Figure 3.5: *Option 4 of the Uranus-Miranda orbiter*

option one stands out. When considering accuracy, the sensor's and pointing ability of the configurations are taken into account. Due to a higher performing sensor, option number two was leading in this category. The reliability of the configuration is determined by taking into consideration the lifetime of the components and their approximate failure-rate. Here, all options are performing sufficiently, but option two and four are rated worse, due to lower number of thrusters or the lack of any RW. As it is found in Table 3.13, the highest rated option is option one. This trade-off and the reasoning behind it is sufficient to select the option one to be the final ADCS sub-system design choice.

4

Integration and Design

For the sensors and actuators of the ADCS sub-system to function properly, they have to be adequately integrated with the rest of the S/C and its other sub-systems. Section 4.1 describes the physical integration of ADCS elements, delving into their placement on the S/C structure and offering improvements compared to the ones specified in WP2 [3]. Subsequently, Section 4.2 will present ADCS architecture, describing in detail how different elements of ADCS interact with each other. Furthermore it explores ADCS software - feedback loops, filtering and control algorithms. Afterwards, electrical power, data transmission and propellant supply interfaces are briefly considered in Section 4.3.

4.1. Comparison of Previous and Updated ADCS Configurations

In WP2 [3], the ADCS configuration consisted of 1 Sun sensor, 2 star sensors, 2 gyroscopes, 4 reaction wheels, and 12 thrusters. The Sun sensor was placed on one of the panels in the pitch/right wing direction. One of the star sensors was mounted on the same panel as the Sun sensor, while the other one was pointed in the roll/velocity direction. The gyroscopes were placed on a hidden layer inside the spacecraft, parallel to its base. The reaction wheels were mounted next to the gyroscopes, three in orthogonal directions and one in an axis, which is the combination of the other three. The thrusters were split into two groups of six, placed in the planes of the top and bottom sides of the spacecraft.

Since the orbit of Uranus is significantly larger than that of Earth, the Sun sensor can be placed facing in the same direction as the hyperbolic antenna since the direction towards the Sun is roughly the same. The three star sensors shall be mounted at 90° angles with respect to each other, on the side opposite no the nadir direction. Four gyroscopes are positioned as close as possible to the S/C's centre of mass, three of them perpendicular to each other and a fourth one making a 45° angle with the rest. As for the actuators, 12 thrusters are placed at different location around the S/C, ensuring balanced moment arms and control around every axis. Lastly, 2 control moment gyros shall be mounted in alignment with the main axis of the spacecraft.

4.2. ADCS Architecture

In order to accurately determine its position and attitude in space, the S/C requires appropriate software, in addition to sufficient sensor systems, to analyse sensor data and transform it into attitude and position.

For the Uranus - Miranda Orbiter ADCS architecture, inspiration has been taken from Cassini-Hyugens attitude control system, which is reported to have performed superbly over its almost 20 years long lifespan [43]. ADCS architecture diagram for UMO, including both hardware and software elements, is presented in Figure 4.1.

Propulsion Sub-system

While the propulsion sub-system is not a part of the ADCS, it has a direct effect on its performance. For example, the largest disturbance torques were estimated to be due to main engine misalignment. As such, propulsion sub-system is an important component of the ADCS architecture.

Space Environment

Space environment includes factors that contribute to disturbances, such as the atmosphere or the gravitational and magnetic fields of Uranus. Additionally, space environment covers sensor inputs, specifically the relative position and distance to the Sun and stars.

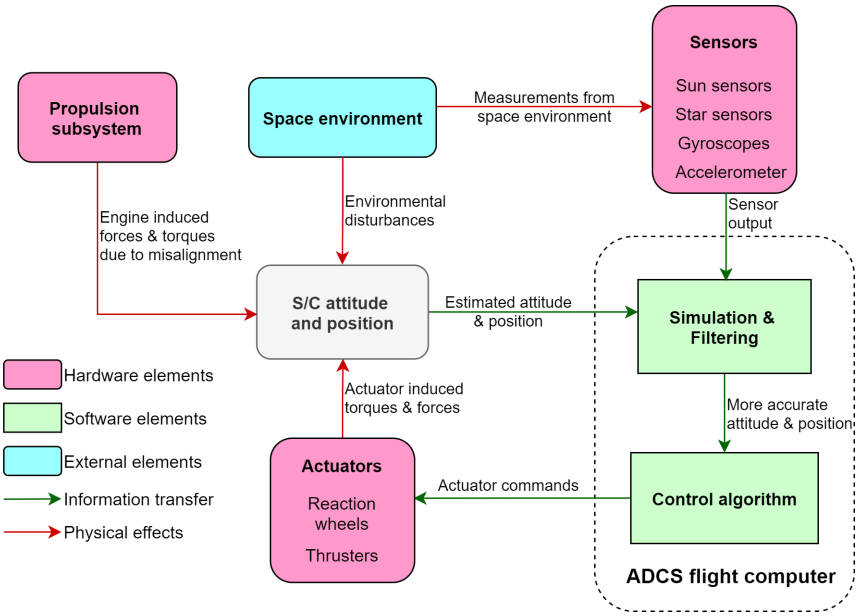

Figure 4.1: *ADCS architecture diagram*

Sensors

Sensors include all ADCS elements that provide the ADCS flight computer with data used to determine the S/C attitude and position. For Uranus-Miranda Orbiter a set of star sensors, Sun sensors, laser gyroscopes and accelerometers have been chosen in Section 3.1. It is unavoidable that these sensors pick up noise, which reduces measurement accuracy, and has to be reduced using filtering software.

S/C Attitude and Position

Spacecraft attitude and position is directly influenced by the space environment, propulsion sub-system and actuators. Main function of ADCS is to control and maintain S/C attitude to allow other sub-systems and the payload to function properly.

Actuators

Actuators are active elements of ADCS that can directly provide the S/C with the necessary torques. Actuators include a wide variety of components, such as reaction/momentum wheels, thrusters or magnetic torquers. For Uranus-Miranda Orbiter, a set of 4 reaction wheels and 12 thrusters have been chosen as actuators in Section 3.2.

Simulation & Filtering

In order to reduce the noise collected by ADCS sensors, measured data is usually manipulated by a version of the Kalman filter, instead of influencing control algorithms directly. A Kalman filter is a recursive algorithm which stores the previous state - attitude and position - of the S/C and makes a prediction of the current state based on a mathematical model. The measurements are then made and compared with the predictions, to create a more accurate estimation of the state of the S/C. This state estimation is then used as input for mathematical model prediction in the next iteration, creating an information feedback loop [44].

Kalman filter algorithm does not require storing more than one previous state, and as such is not demanding on ADCS flight computer RAM. However, a trade-off between model algorithm accuracy and flight computer computational capacity requirement has to be made when choosing the time-step between Kalman filter iterations. Lower time-step means more state updates in a given time frame, which increases accuracy, however increases processing power of ADCS flight computer, increasing both its electrical power requirement and necessary mass. For now, a range of 1 s to 5 s will be considered for time-step, a value taken from Cassini space mission [43]. However, consideration of advancements in computer processor technology might allow reduction of filter time-step without significant adverse effects.

Kalman filter has numerous sub-types, each with different applications. For S/C ADCS, either Kalman-Bucy filter [43], (Robust) Extended Kalman filter or (Robust) Unscented Kalman filter are used [45].

Control Algorithm

Control algorithm takes as input S/C attitude and position estimated in Simulation & Filtering and provides precise commands to actuators to either maintain current attitude or perform slew manoeuvres depending on S/C requirements.

4.3. ADCS Interfaces

For successful operation of ADCS, sufficient electrical power, as well as communication between different ADCS components has to be ensured. A diagram displaying electrical power, data transfer and propellant flow interfaces of ADCS elements is presented in Figure 4.2.

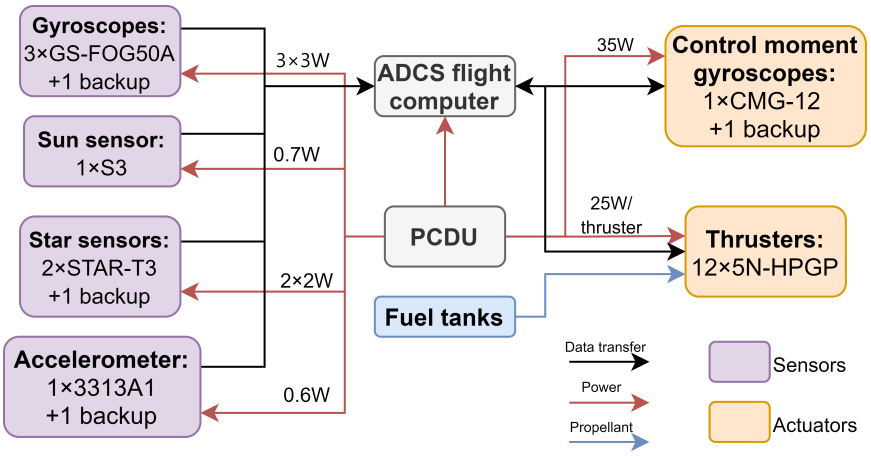

Figure 4.2: *ADCS elements interface diagram*

Electrical power is distributed to the ADCS sensors and actuators directly from the Power Conditioning and Distribution Unit (PCDU), described in WP2 [3]. Cables used to connect the ADCS components to the PCDU shall have as low electrical resistance as possible to reduce power losses and the connection interfaces between cables and components or the PCDU shall be able to withstand loads and vibrations experienced during launch and mission.

Sensor data analysis and actuator command is managed by the ADCS flight computer which collects data from sensors, runs Kalman filter estimations and, based on control algorithms, activates or deactivates the corresponding actuators. Cables connecting the ADCS computer and the sensors shall be capable of ensuring sufficient data-rate without significant power lost and without unnecessary heat emissions. Additionally, cable connections shall be able to withstand loads and vibrations during launch and missions.

Furthermore, care must be taken to minimise induced magnetic field when arranging cables within the S/C, since internal magnetic fields can negatively affect other electrical components and create additional noise for the ADCS sensors or payload instruments.

Additionally, the ADCS interfaces include the thruster propellant supply system. The pipe system connecting thrusters and propellant tanks shall be able to provide thrusters with sufficient propellant mass flow. Moreover, pipe connectors shall be able to withstand loads experienced by the spacecraft, and no leaks can be present in propellant supply system.

It must be noted that power requirements of both sensors and actuators are known and presented in Figure 4.2. However, data rate of sensors and propellant flow of actuators are not provided and have to be specified from the manufacturers before complete ADCS interfaces can be designed in detail. Additionally, since sensor data rate is unknown and ADCS software has not been developed, computing performance, electrical power, storage and random access memory (RAM) requirements of the ADCS flight computer are not determined in this report.

5

Conclusion & Recommendations

The purpose of this study is to do a second iteration of the Attitude Determination and Control System (ADCS) sub-system, with more detailed calculations and designs. Furthermore, the integration of this particular sub-system within the S/C will also be discussed.

Firstly, the disturbance torques that will affect the S/C were calculated in Chapter 2, together with proposed recommendations on the design of the S/C made in WP2 [3] that will reduce the effect of those torques. Some of the recommendations included placing the fuel tanks closer to the structure-s centre of mass or using sensors and actuators that require the least volume possible.

Later on, in Chapter 3, different sensors and actuators together with their properties were discussed. After the model of each possible sensor and actuator had been chosen in Section 3.1 and Section 3.2, possible configurations of each that ensured full redundancy were proposed and a final configuration was selected after a trade-off in Section 3.3. The final configuration included one Sun sensor, three star sensors, four gyroscopes and two accelerometers for the sensors and two CMG and twelve thrusters for the actuators.

Once all calculations and recommendations were done, the integration of the ADCS sub-system with the rest of the S/C was discussed in Chapter 4, including a detailed sub-system architecture diagram. However, the data-rate required by the sensors and the propellant flow of the actuators were not specified and thus a detailed interface could not be designed.

It is recommended to designed a detailed interface as soon as the data rate required by the sensors and the propellant flow rate are known, and to then test the S/C with torques higher than those expected in order to confirm the accuracy of all calculations made. Then, if the result of these tests was not satisfactory, another iteration of the design could be made.

Bibliography

[1] N., F. L., Fletcher, L. N., Simon, A. A., Hofstadter, M. D., Arridge, C. S., Cohen, I. J., Masters, A., Mandt, K., and Coustenis, A., "Ice giant system exploration in the 2020s: An introduction," , Nov 2020. URL https://royalsocietypublishing.org/doi/10.1098/rsta.2019.0473.

[2] Garcia, J. A., Gorovojs, D., Mazur, B., Oppelaar, J., Ganapathy, K., Maximchuk, M., Olimid, D., and Welters, S., "Uranus-Miranda Initial Sizing - WP1 - C09," , 2021. This is the first WP delivered.

[3] Garcia, J. A., Gorovojs, D., Mazur, B., Oppelaar, J., Ganapathy, K., Maximchuk, M., Olimid, D., and Welters, S., "Uranus-Miranda Orbiter Desgin: Subsystem Design - WP2 - C09," , 2021. This is the second WP delivered.

[4] n.a., n.d.. URL https://ai-solutions.com/_freeflyeruniversityguide/attitude_reference_frames.htm.

[5] Williams, D., "Uranus Fact Sheet," , Nov 2020. URL https://nssdc.gsfc.nasa.gov/planetary/factsheet/uranusfact.html.

[6] Zandbergen, B., *Aerospace Design & Systems Engineering Elements I*, 2021. ADSEE-I reader.

[7] Larson, W. J., and Wertz, J. R., *Space mission analysis and design*, 3rd ed., Kluwer Academic Publishers, 2005.

[8] Czernia, D., "Mass Moment of Inertia Calculator," , Jul 2018. URL https://www.omnicalculator.com/physics/mass-moment-of-inertia#moment-of-inertia-equation.

[9] Hibbeler, R. C., *Engineering Mechanics in SI Units*, 14th ed., Vol. Statics, Pearson Education Limited, 2017.

[10] Ramnath, R. V., *Computation and Asymptotics*, Springer Berlin Heidelberg, 2012. doi:10.1007/978-3-642-25749-0, URL https://doi.org/10.1007/978-3-642-25749-0.

[11] Howard, S., "Uranus and Neptune Revisited," *Journal. Washington Academy of Sciences, Washington, D. C*, 2015.

[12] Fortescue, P. W., Stark, J., and Swinerd, G., *Spacecraft systems engineering*, 3rd ed., J. Wiley, 2003.

[13] Eyerman, C. E., "A Systems Engineering Approach to Disturbance Minimization for Spacecraft Utilizing Controlled Structures Technology," Master's thesis, Massachusetts Institute of Technology, Jun 1990.

[14] Cervone, A., "Lecture S2: Spacecraft Attitude Determination & Control System," , Sep 2021.

[15] Prakash, R., "Angular momentum and angular impulse review," , n.d. URL https://www.khanacademy.org/science/in-in-class-11-physics-cbse-hindi/in-in-11-system-of-particles-and-rotational-motion-hindi/angular-momentum-and-angular-impulse-ha/angular-momentum-ap-physics-1.

[16] staff, S.-P. . D.-T., "Margin Philosophy for science assessment studies," , Jun 2012. URL https://sci.esa.int/documents/34375/36249/1567260131067-Margin_philosophy_for_science_assessment_studies_1.3.pdf.

[17] Nosseir, A. E. S., Cervone, A., and Pasini, A., "Review of State-of-the-Art Green Monopropellants: For Propulsion Systems Analysts and Designers," *Aerospace*, Vol. 8, No. 1, 2021, p. 20. doi:10.3390/aerospace8010020, URL https://doi.org/10.3390/aerospace8010020.

[18] Cervone, A., "Lecture S1: Spacecraft Attitude Determination & Control System," , Sep 2021.

[19] Engineering, O., "How to measure acceleration?" , Mar 2021. URL https://www.omega.com/en-us/resources/accelerometers#:~:text=An%20accelerometer%20is%20a%20device,the%20force%20exerted%20upon%20it.

[20] "Star Trackers," , Jul 2020. URL https://www.vectronic-aerospace.com/star-trackers/.

[21] "STAR-T3," , Sep 2021. URL https://satsearch.co/products/space-inventor-star-t3.

[22] "S3 (Smart Sun Sensor)," , 2021. URL https://satsearch.co/products/leonardo-finmeccanica-smart-sun-sensor.

[23] "Mini Fine Sun Sensor," , 2021. URL https://satsearch.co/products/bradford-mini-fine-sun-sensor.

[24] "Fine Sun Sensor," , 2021. URL https://satsearch.co/products/bradford-fine-sun-sensor.

[25] "GS-FOG50A Closed-Loop Fiber Optic Gyroscope," , Sep 2021. URL https://satsearch.co/products/gnssmart-gs-fog50a-gyroscope.

[26] "GS-FOG60A Closed-Loop Fiber Optic Gyroscope," , Sep 2021. URL https://satsearch.co/products/gnssmart-gs-fog60a-gyroscope.

[27] "GS-FOG70A Closed-Loop Fiber Optic Gyroscope," , Sep 2021. URL https://satsearch.co/products/gnssmart-gs-fog70a-gyroscope.

[28] "3313 Series Triaxial Accelerometer," , 2020. URL https://satsearch.co/products/dytran-3313-series-triaxial-accelerometer.

[29] "GS-JBK-9 Precision Quartz Flexure Accelerometer," , 2021. URL https://satsearch.co/products/gnssmart-gs-jbk-9-accelerometer.

[30] Jafari, M., "Optimal redundant sensor configuration for accuracy increasing in space inertial navigation system," *Aerospace Science and Technology*, Vol. 47, 2015, pp. 467–472. doi:10.1016/j.ast.2015.09.017, URL https://doi.org/10.1016/j.ast.2015.09.017.

[31] SatCatalog, "HR16-75," , 2020. URL https://www.satcatalog.com/component/hr16-75/.

[32] SatCatalog, "RWA-15," , 2020. URL https://www.satcatalog.com/component/rwa-15/.

[33] "Reaction Wheel VRW-D-4," , Jan 2021. URL https://www.vectronic-aerospace.com/wp-content/uploads/2020/06/VAS-VRWD4-DS2.pdf.

[34] "Smallsat Reaction Wheel Cluster (RC4-17.0)," , 2019. URL https://satcatalog.s3.amazonaws.com/components/245/SatCatalog_-_Sinclair_Interplanetary_-_RC4-17.0_-_Datasheet.pdf.

[35] "RW1000 Large Reaction Wheel," , 2020. URL https://satcatalog.s3.amazonaws.com/components/243/SatCatalog_-_OCE_Technology_-_RW1000_-_Datasheet.pdf.

[36] Kovo, Y., "4.0 in-space propulsion," , Mar 2020. URL https://www.nasa.gov/smallsat-institute/sst-soa-2020/in-space-propulsion.

[37] Wilson, F., "In-Space Propulsion Data Sheets," , Aug 2020. URL https://www.rocket.com/sites/default/files/documents/In-Space%20Data%20Sheets%204.8.20.pdf.

[38] Cortés-Borgmeyer, S., "1n hydrazine thruster," , n.d. URL https://www.space-propulsion.com/spacecraft-propulsion/hydrazine-thrusters/1n-hydrazine-thruster.html.

[39] n.a., "PDF," , 2018. URL https://www.moog.com/content/dam/moog/literature/Space_Defense/spaceliterature/propulsion/Moog-MonopropellantThrusters-Datasheet.pdf.

[40] n.a., "Enabling High Performance Green Propulsion for SmallSats," , Aug 2015. URL https://digitalcommons.usu.edu/cgi/viewcontent.cgi?article=3240&context=smallsat.

[41] n.a., "5N HPGP thruster," , n.d.. URL https://www.ecaps.space/products-5n.php.

[42] n.a., "BGT-X5: Green Monopropellant Thruster," , 2021. URL https://static1.squarespace.com/static/60df2bfb6db9752ed1d79d44/t/61292af2a097083a87c4cbc0/1630087925107/BGT_X5_v1.0.pdf.

[43] Lee, A. Y., and Burk, T. A., *Cassini Spacecraft Attitude Control System: Flight Performance and Lessons Learned*, California Institute of Technology, 2017.

[44] Kim, Y., and Bang, H., "Introduction to Kalman Filter and Its Applications," *Introduction and Implementations of the Kalman Filter*, IntechOpen, 2019, p. /. doi:10.5772/intechopen.80600, URL `https://doi.org/10.5772/intechopen.80600`.

[45] Soken, H. E., Hajiyev, C., and ichiro Sakai, S., *Robust Kalman filtering for small satellite attitude estimation in the presence of measurement faults*, Elsevier Ltd., 2013.

A

General Drawing of the Uranus Miranda Orbiter

In this appendix, the general CATIA drawings are presented. Figure A.1 and Figure A.2 are the first and second sheet of the drafting respectively.

Bill of Material: UMO-GEN-EXT

Number	Quantity	Part Number	Type	Nomenclature	Revision
	1	UMO-STR-MAIN	Assembly	Structure Subsystem	A
	1	UMO-PRO-SA1	Assembly	Propulsion subsystem	A
	1	UMO-GEN-LAY1	Assembly	Basic Layout S/C	A
12	14	UMO-THE-LOUVRE	Part	Thermal Control Louvre	A
1	1	UMO-TTC-HGANT	Part	High gain parabolic dish	A
	1	UMO-CONF-3STAR	Assembly	Three stars configuration	A
7	12	UMO-ADCS-THR	Part	ADCS Thruster	A
13	1	UMO-ADCS-SUN	Part	Sun Sensor	A
3	1	UMO-PLD-HR250	Part	High Resolution Visible Camera	A
5	1	UMO-PLD-TIS	Part	Thermal Infrared Sensor	A
2	1	UMO-PLD-EPT	Part	Radiation Monitor	A
6	1	UMO-PLD-VIMS	Part	Visible and near Infrared Multi-wavelength Spectrometer	A
4	1	UMO-PLD-ORBITER	Part	Miranda Orbiter	A

Bill of Material: UMO-STR-MAIN

Number	Quantity	Part Number	Type	Nomenclature	Revision
15	2	UMO-Structures-Octagon	Part	Structure Octagon Base	A
	4	UMO-Structure-WallAssembly	Assembly	Structure Wall	A
	4	UMO-Structure-WallAssembly	Assembly	Structure Wall	A
16	3	UMO-STR-ASRG_MNT	Part	Structure ASRG Mount	A
17	9	UMO-STR-1494LTANK	Part	1494L Propellant Tank	A
18	1	UMO-STR-389LTANK	Part	389L Propellant Tank	A
19	1	UMO-STR-169LTANK	Part	169L Propellant Tank	A
21	3	UMO-THE-ASRG	Part	ASRG	B
22	4	UMO-STR-COL	Part	Structure Column	A
	2	UMO-STR-15LTANK	Part	15L Propellant Tank for ADCS	A

Bill of Material: UMO-Structure-WallAssembly

Number	Quantity	Part Number	Type	Nomenclature	Revision
23	1	UMO-Structure-Wall	Part	Structure Wall	A
24	1	UMO-Structure-Stringer	Part	Structure Stringer	A

Bill of Material: UMO-Structure-WallAssembly

Number	Quantity	Part Number	Type	Nomenclature	Revision
23	1	UMO-Structure-Wall	Part	Structure Wall	A
25	1	UMO-Structure-Stringer	Part	Structure Stringer	A

Bill of Material: UMO-PRO-SA1

Number	Quantity	Part Number	Type	Nomenclature	Revision
26	1	UMO-PRO-NZLE	Part	Engine nozzle, compustion chamber	A
27	1	UMO-PRO-VLVS	Part	Engine Pumps and Valves	A
28	1	UMO-PRO-PCA	Part	Pressure control assembly	A
29	1	UMO-PRO-PIA	Part	Pressure isolation assembly	A
30	2	UMO-PRO-SEN	Part	Propulsion subsystem sensor	A

Bill of Material: UMO-GEN-LAY1

Number	Quantity	Part Number	Type	Nomenclature	Revision
31	1	UMO-STR-FLOOR	Part	Structure floor	A
32	4	UMO-THE-RHU	Part	Radioisotope heater unit	A
37	1	UMO-CDH-BOX	Part	CDH Command Box	A
38	1	UMO-TTC-BOX	Part	CDH Command Box	A
	1	UMO-CONF-4GYROS	Assembly	Four gyroscopes assembly	A

Bill of Material: UMO-CONF-4GYROS

Number	Quantity	Part Number	Type	Nomenclature	Revision
	4	UMO-ADCS-G50	Part	Gyroscope	A

Bill of Material: UMO-CONF-3STAR

Number	Quantity	Part Number	Type	Nomenclature	Revision
	3	UMO-ADCS-A1	Part	Star sensor	A
	1	UMO-CONF-STARPLATE	Part	Suporting element for three star sensors	A

Recapitulation of: UMO-GEN-EXT
Different parts: 32
Total parts: 95

Quantity	Part Number
2	UMO-Structures-Octagon
8	UMO-Structure-Wall
4	UMO-Structure-Stringer
4	UMO-Structure-Stringer
3	UMO-STR-ASRG_MNT
9	UMO-STR-1494LTANK
1	UMO-STR-389LTANK
1	UMO-STR-169LTANK
3	UMO-THE-ASRG
4	UMO-STR-COL
2	UMO-STR-15LTANK
1	UMO-PRO-NZLE
1	UMO-PRO-VLVS
1	UMO-PRO-PCA
1	UMO-PRO-PIA
2	UMO-PRO-SEN
1	UMO-STR-FLOOR
4	UMO-TC-RHU
1	UMO-CDH-BOX
1	UMO-TTC-BOX
4	UMO-ADCS-G50
14	UMO-THE-LOUVRE
1	UMO-TTC-HGANT
3	UMO-ADCS-A1
1	UMO-CONF-STARPLATE
12	UMO-ADCS-THR
1	UMO-ADCS-SUN
1	UMO-PLD-HR250
1	UMO-PLD-TIS
1	UMO-PLD-EPT
1	UMO-PLD-VIMS
1	UMO-PLD-ORBITER

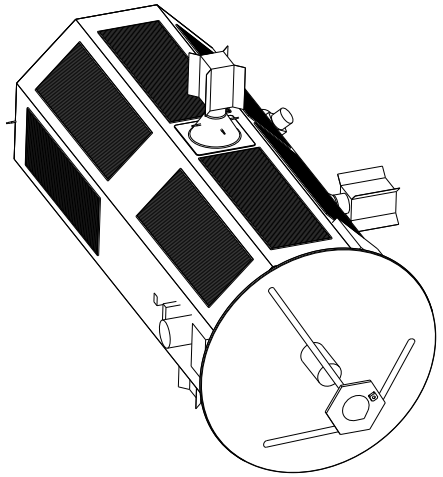

Isometric view
Scale: 1:25

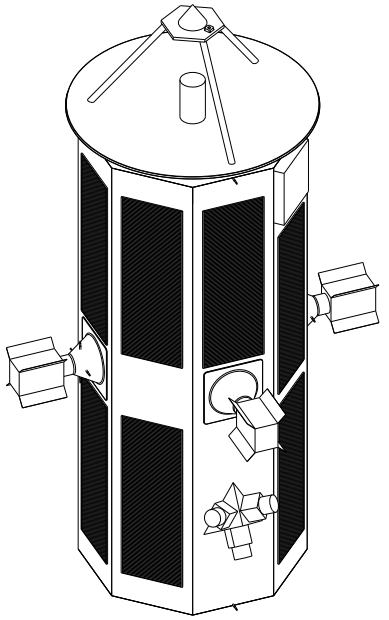

Isometric view
Scale: 1:25

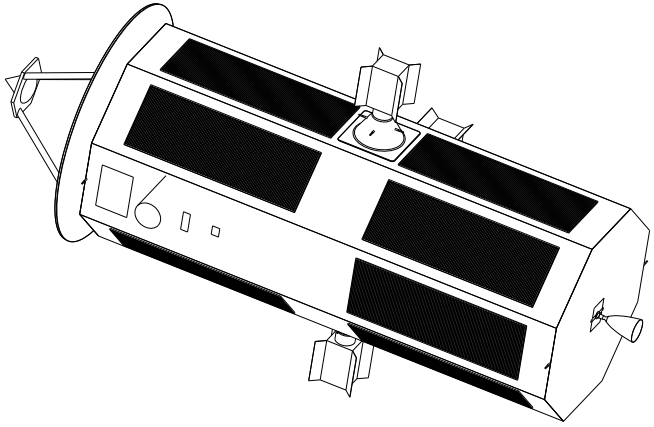

Isometric view
Scale: 1:25

This drawing is our property. It can't be reproduced or communicated without our written agreement.

DASSAULT SYSTEMES

DRAWING TITLE: Uranus-Miranda Orbiter Assembly

DRAWN BY: Dominic	DATE: 04/02/2021	SIZE: A0	DRAWING NUMBER: UMO-GEN-EXT
CHECKED BY: Sebastian	DATE: 04/10/2021		REV: A
DESIGNED BY: Mikhail	DATE: 04/15/2021	SCALE: 1:40	WEIGHT(kg):289.37
			SHEET: 1/2

Figure A.1: *Bill of materials and isometric view of the general layout of the Uranus Miranda Orbiter*

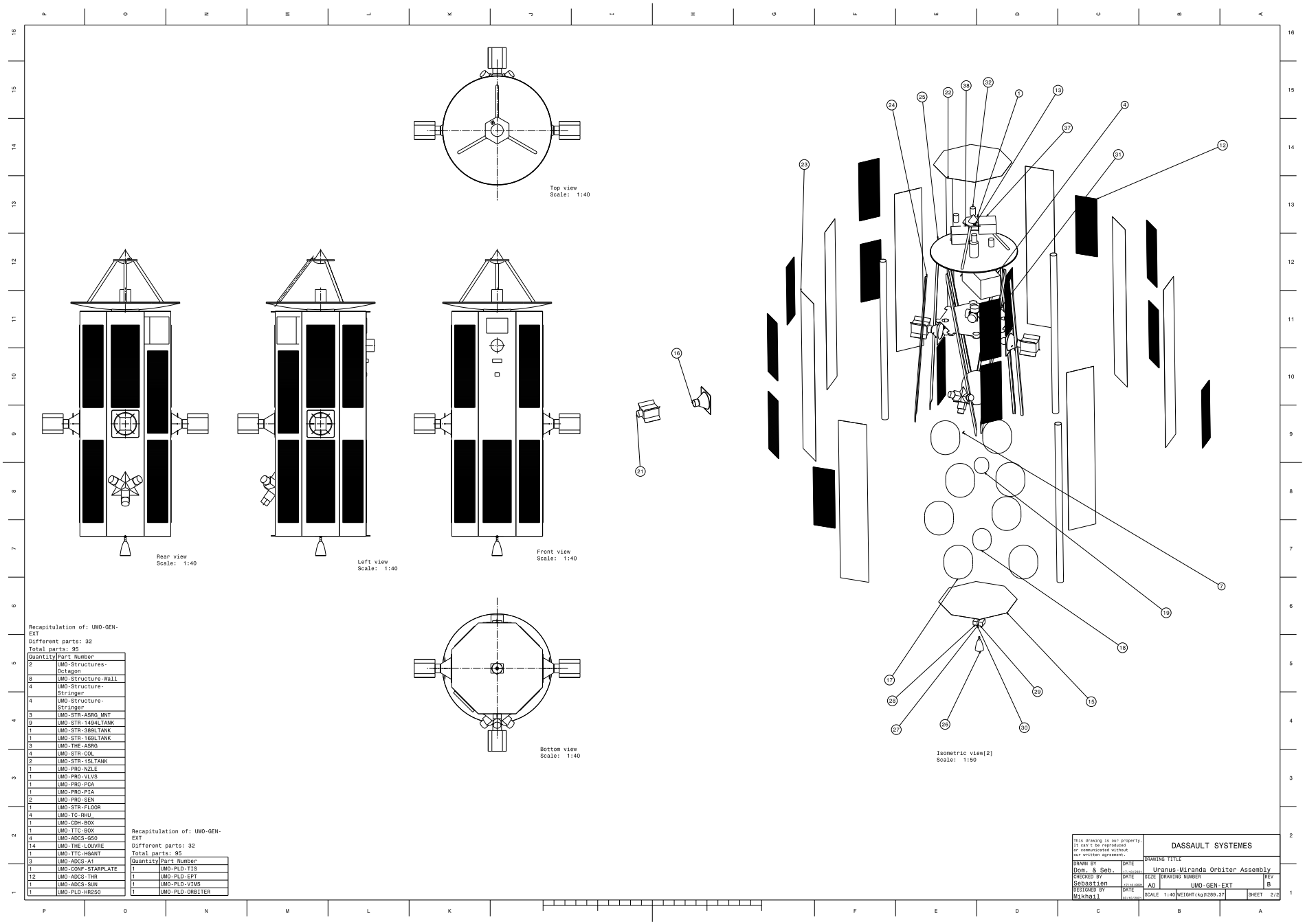

Figure A.2: *3 view projection and exploded view of the general layout of the Uranus Miranda Orbiter*

B

Python scripts for ADCS torques, angular impulse and propellant mass calculations

In this appendix, the python script made to calculate the disturbance torques, angular impulses and propellant mass are presented. This file is dependant of an input parameter file but due to the page restriction on this report, it is not inserted. The files can be requested from Sébastien José Welters. If he is not available, please contact other group members.

```python
import input_parameters as ip
import numpy as np
from scipy.integrate import quad


def COM(masses):
    mass_array = np.array([0, 0, 0, 0])
    for v in masses:
        mass_array = np.vstack((mass_array, v))
    c_mass = np.average(mass_array[:, :3], axis=0, weights=mass_array[:, 3])
    c_mass[:3] += ip.CG_uncertainty
    return c_mass


# def COP(areas):
#     area_array = np.array([0, 0, 0, 0])
#     for v in areas:
#         area_array = np.vstack((area_array, v))
#     c_pressure = np.average(area_array[:, :3], axis=0, weights=area_array[:, 3])
#     return c_pressure


cm_array_init = COM(ip.masses_init)
cm_array_fin = COM(ip.masses_fin)
cm_array_avg = (cm_array_init + cm_array_fin) / 2

v_mission = np.array([ip.v_orbit, 0, 0])


# # # Base Equations External Disturbances # # #

def aerodynamic_torque(r_m, v):
    F_a = 0.5 * ip.rho * ip.C_d * np.square(v) * ip.S
    torque = np.cross(r_m, F_a)
    return torque


def solar_torque(r_p):
    F_s = (1 + ip.rho_opt) * ip.P_s_uranus * ip.S
    torque = np.cross(r_p, F_s)

    return torque
```

```
43
44
45  def gravity_torque(I_x, I_y, I_z, phi, theta):
46      grav_tor_x = 3 / 2 * ip.n_sq * (abs(0.99*I_y - I_z) * np.sin(2 * phi) *
        ↪  np.square(np.cos(theta)))
47      grav_tor_y = 3 / 2 * ip.n_sq * (abs(I_x - I_z) * np.sin(2 * theta) * np.cos(phi))
48      grav_tor_z = 3 / 2 * ip.n_sq * (abs(I_x - I_y) * np.sin(phi) * np.sin(2 * theta))
49      torque = np.array([grav_tor_x, grav_tor_y, grav_tor_z])
50      return torque
51
52
53  def magnetic_torque(D, B):
54      torque = D * B
55      torque_array = np.array([1/3, 1/3, 1/3])*torque
56      return torque_array, torque
57
58
59  # # # Variable Equations External Disturbances # # #
60
61  def torque_ae_x_var(t):
62      k2 = cm_array_avg[2] * 0.5 * ip.C_d * ip.rho * np.square(ip.v_orbit) * ip.S[1]
63
64      return - k2 * np.square(np.sin(ip.omega * t))
65
66
67  def torque_ae_y_var(t):
68      k1 = cm_array_avg[2] * 0.5 * ip.C_d * ip.rho * np.square(ip.v_orbit) * ip.S[0]
69
70      return k1 * np.square(np.cos(ip.omega * t))
71
72
73  def torque_ae_z_var(t):
74      k1 = cm_array_avg[0] * 0.5 * ip.C_d * ip.rho * np.square(ip.v_orbit) * ip.S[1]
75      k2 = cm_array_avg[1] * 0.5 * ip.C_d * ip.rho * np.square(ip.v_orbit) * ip.S[0]
76
77      return k1 * np.square(np.sin(ip.omega * t)) - k2 * np.square(np.cos(ip.omega * t))
78
79
80  def torque_s_x_var(t):
81      k2 = cm_array_avg[2] * (1 + ip.rho_opt) * ip.P_s_uranus * ip.S[1]
82
83      return - k2 * np.cos(ip.omega * t)
84
85
86  def torque_s_y_var(t):
87      k1 = cm_array_avg[2] * (1 + ip.rho_opt) * ip.P_s_uranus * ip.S[0]
88
89      return k1 * np.sin(ip.omega * t)
90
91
92  def torque_s_z_var(t):
93      k1 = cm_array_avg[0] * (1 + ip.rho_opt) * ip.P_s_uranus * ip.S[1]
94      k2 = cm_array_avg[1] * (1 + ip.rho_opt) * ip.P_s_uranus * ip.S[0]
95
96      return k1 * np.sin(ip.omega * t) - k2 * np.cos(ip.omega * t)
97
98
99  def torque_grav_x_var(t):
100     k1 = 3 / 2 * ip.n_sq * abs(0.99*ip.I_yy - ip.I_zz) * np.sin(2*ip.phi_misalignment)
101
```

```
    return k1 * np.square(np.cos(ip.omega * t))


def torque_grav_y_var(t):
    k1 = 3 / 2 * ip.n_sq * abs(ip.I_xx - ip.I_zz) * np.cos(ip.phi_misalignment)

    return k1 * np.sin(2 * ip.omega * t)


def torque_grav_z_var(t):
    k1 = 3 / 2 * ip.n_sq * abs(ip.I_xx - ip.I_yy) * np.sin(ip.phi_misalignment)

    return k1 * np.square(np.sin(ip.omega * t))


# # # Base Equations Internal Disturbances # # #

def thrust_misalignment():
    torque = ip.arm_thrust_misalignment_array * ip.thrust_mainengine
    impulse_array = torque * ip.burn_time_mainengine

    return torque, impulse_array


# # # Main Function All Disturbances # # #

def impulse_all_per_orbit():

    # # # External Angular Impulses # # #

    # # Aerodynamic Angular Impulse # #
    impulse_ae_mission = aerodynamic_torque(cm_array_avg, v_mission) * (3/4*ip.t_orbit -
    ↪  ip.t_orbit_before_90deg_sun)
    impulse_ae_sending_x = np.abs(quad(torque_ae_x_var, -ip.t_orbit_before_90deg_sun,
    ↪  0)[0]) + \
                           np.abs(quad(torque_ae_x_var, 0, ip.t_orbit/4)[0])
    impulse_ae_sending_y = np.abs(quad(torque_ae_y_var, -ip.t_orbit_before_90deg_sun,
    ↪  0)[0]) + \
                           np.abs(quad(torque_ae_y_var, 0, ip.t_orbit/4)[0])
    impulse_ae_sending_z = np.abs(quad(torque_ae_z_var, -ip.t_orbit_before_90deg_sun,
    ↪  0)[0]) + \
                           np.abs(quad(torque_ae_z_var, 0, ip.t_orbit/4)[0])
    impulse_ae_sending = np.array([impulse_ae_sending_x, impulse_ae_sending_y,
    ↪  impulse_ae_sending_z])
    impulse_ae = np.abs(impulse_ae_mission) + np.abs(impulse_ae_sending)

    # # Solar Angular Impulse # #
    impulse_solar_sending = solar_torque(cm_array_avg) * (ip.t_orbit_before_90deg_sun +
    ↪  ip.t_orbit/4)
    impulse_solar_mission_day_x = np.abs(quad(torque_s_x_var, ip.t_orbit/4,
    ↪  ip.t_orbit/2)[0]) + \
                                  np.abs(quad(torque_s_x_var, ip.t_orbit/2,
                                  ↪  ip.t_orbit/2+ip.t_orbit_before_90deg_sun)[0])
    impulse_solar_mission_day_y = np.abs(quad(torque_s_y_var, ip.t_orbit/4,
    ↪  ip.t_orbit/2)[0]) + \
                                  np.abs(quad(torque_s_y_var, ip.t_orbit/2,
                                  ↪  ip.t_orbit/2+ip.t_orbit_before_90deg_sun)[0])
    impulse_solar_mission_day_z = np.abs(quad(torque_s_z_var, ip.t_orbit/4,
    ↪  ip.t_orbit/2)[0]) + \
```

```
                                np.abs(quad(torque_s_z_var, ip.t_orbit/2,
                                    ip.t_orbit/2+ip.t_orbit_before_90deg_sun)[0])
    impulse_solar_mission_day = np.array([impulse_solar_mission_day_x,
    impulse_solar_mission_day_y, impulse_solar_mission_day_z])
    impulse_solar = np.abs(impulse_solar_mission_day) + np.abs(impulse_solar_sending)

    # # Gravity Angular Impulse # #
    impulse_grav_mission = gravity_torque(ip.I_xx, ip.I_yy, ip.I_zz,
    ip.theta_misalignment, ip.phi_misalignment) * \
                           (3/4*ip.t_orbit - ip.t_orbit_before_90deg_sun)
    impulse_grav_sending_x = np.abs(quad(torque_grav_x_var, -ip.t_orbit_before_90deg_sun,
    0)[0]) + \
                             np.abs(quad(torque_grav_y_var, 0, ip.t_orbit/4)[0])
    impulse_grav_sending_y = np.abs(quad(torque_grav_y_var, -ip.t_orbit_before_90deg_sun,
    0)[0]) + \
                             np.abs(quad(torque_grav_y_var, 0, ip.t_orbit/4)[0])
    impulse_grav_sending_z = np.abs(quad(torque_grav_z_var, -ip.t_orbit_before_90deg_sun,
    0)[0]) + \
                             np.abs(quad(torque_grav_z_var, 0, ip.t_orbit/4)[0])
    impulse_grav_sending = np.array([impulse_grav_sending_x, impulse_grav_sending_y,
    impulse_grav_sending_z])
    impulse_grav = np.abs(impulse_grav_mission) + np.abs(impulse_grav_sending)

    impulse_magnetic_mission = magnetic_torque(ip.D, ip.B_uranus)[0] * ip.t_orbit

    # # # Repositioning Angular Momentum # # #
    impulse_rotation_sending = ip.I_yy * ip.omega
    impulse_stop_rotation = impulse_rotation_sending
    impulse_rotation = np.abs(impulse_stop_rotation) + np.abs(impulse_stop_rotation)
    # Not included in sum because rotation wheel can initialize the rotation and end it
    without needing the thrusters

    # # # Internal Angular Impulse # # #

    impulse_thrust_mainengine = thrust_misalignment()[1]/ip.n_orbits

    # # # Sum # # #

    sum_impulse_ext_array = impulse_ae + impulse_solar + impulse_grav +
    impulse_magnetic_mission
    sum_impulse_ext = np.sum(sum_impulse_ext_array)

    sum_impulse_int_array = impulse_thrust_mainengine
    sum_impulse_int = np.sum(sum_impulse_int_array)

    sum_impulse_tot_array = sum_impulse_ext_array + sum_impulse_int_array
    sum_impulse_tot = np.sum(sum_impulse_tot_array)

    return {
        "Impulse due to aerodynamics during mission": impulse_ae_mission,
        "Impulse due to aerodynamics during sending": impulse_ae_sending,
        "Impulse due to solar during mission day": impulse_solar_mission_day,
        "Impulse due to solar during sending": impulse_solar_sending,
        "Impulse due to rotation to rotate for sending": impulse_rotation,
        "Impulse due to gravity during mission": impulse_grav_mission,
        "Impulse due to gravity during sending": impulse_grav_sending,
        "Impulse due to magnetic field during mission": impulse_magnetic_mission,
        "Impulse due to thrust misalignment during mission": impulse_thrust_mainengine,
        "Total impulse (internal and external)": sum_impulse_tot_array
    }, np.array(sum_impulse_tot_array), sum_impulse_tot
```

```
201
202
203 def propellant_mass(thrust, mdot, impulse_array):
204     t_b_array = impulse_array/(thrust * 2*ip.distance_thrusters_to_cm)
205     m_p_array = mdot * t_b_array
206     t_b_array_margin = ip.propmargin * t_b_array
207     m_p_array_margin = ip.propmargin * m_p_array
208     return m_p_array, t_b_array, m_p_array_margin, t_b_array_margin
209
210
211 ae_torque = aerodynamic_torque(cm_array_avg, v_mission)
212 s_torque = solar_torque(cm_array_avg)
213 grav_torque = gravity_torque(ip.I_xx, ip.I_yy, ip.I_zz, ip.theta_misalignment,
    ↪  ip.phi_misalignment)
214 m_torque = magnetic_torque(ip.D, ip.B_uranus)
215 thrust_misal_torque = thrust_misalignment()[0]
216
217 m_p_tot = np.sum(propellant_mass(ip.thrust_adcs, ip.m_dot_adcs,
    ↪  impulse_all_per_orbit()[1])[0] * ip.n_orbits)
218 t_b_axis_orbit = propellant_mass(ip.thrust_adcs, ip.m_dot_adcs,
    ↪  impulse_all_per_orbit()[1])[1]
219
220 m_p_tot_margin = np.sum(propellant_mass(ip.thrust_adcs, ip.m_dot_adcs,
    ↪  impulse_all_per_orbit()[1])[2] * ip.n_orbits)
221 t_b_axis_orbit_margin = propellant_mass(ip.thrust_adcs, ip.m_dot_adcs,
    ↪  impulse_all_per_orbit()[1])[3]
222 V_p_margin = m_p_tot_margin/ip.propdensity
223
224 # mp_array = []
225 # tb_array = []
226 # for i in range(len(ip.ft)):
227 #     m_p = np.sum(propellant_mass(ip.ft[i], ip.mdot[i], impulse_all_per_orbit()[1])[0] *
    ↪  ip.n_orbits)
228 #     mp_array.append(m_p)
229 #     tb = propellant_mass(ip.ft[i], ip.mdot[i], impulse_all_per_orbit()[1])[1] *
    ↪  ip.n_orbits
230 #     tb_array.append(tb)
231 # print(mp_array)
232 # print(tb_array)
233
234 # print(COM(ip.masses_av))
235
236 # # Print all torques: # #
237 print("The torques are:")
238 print("Aerodynamic torque:", ae_torque, " (non-variable)")
239 print("Solar torque:", s_torque, " (non-variable)")
240 print("Gravity gradient torque:", grav_torque, " (non-variable)")
241 print("Magnetic torque:", m_torque, " (non-variable)")
242 print("Torque created by misalignment of main thruster:", thrust_misal_torque, "
    ↪  (non-variable)")
243
244 print("\n")
245 # # Print Impulses: # #
246 print("All separate angular impulses per orbit:", impulse_all_per_orbit()[0])
247 print("Total angular impulse per orbit array:", impulse_all_per_orbit()[1])
248 print("Total angular impulse per orbit:", impulse_all_per_orbit()[2])
249 print("Total angular impulse during mission:", impulse_all_per_orbit()[2] * ip.n_orbits)
250
251 print("\n")
252 # # Print total propellant mass and burn time per axis (of thruster pair)
```

```
print("Propellant mass for ADCS:", m_p_tot)
print("Burn time array per orbit:", t_b_axis_orbit)
print("Total propellant mass for ADCS with margin:", m_p_tot_margin)
print("Burn time array with margin per orbit:", t_b_axis_orbit_margin)
print("Total propellant volume for ADCS with margin", V_p_margin)
```

C

Task and time distribution

Group C09 time distribution for WP3

Table C.1: *Group C09 task distribution and time spend for WP2*

Chapter	**Names**
1	Javier (2h)
2	Kamalesh (16h) Sebastian ()
3	Jan (14h) Javier (10h) Dominic (14h) Bart (16h)
4	Daniels (8h) Mikhail (8h)
5	Javier (2h)
CATIA	Dominic (11h) Sebastian () Mikhail (11h)
other	Jan (8h) Javier (4h) Bart (8h) Daniels (4h) Dominic (4h) Kamalesh (8h) Sebastian (40h)

Familiarisation - All
Gantt Chart- Sebas

Report writing & Latex

Chapter 2: S/C Parameters and Disturbances

Sections 2.1 to 2.3 and 2.5 - Kamalesh, Sebastien
Section 2.4 - Sebastien

Chapter 3: Sensors and Actuators for Attitude Determination and Control

Section 3.1 - Jan, Javier
Section 3.2 - Bart, Dominic
Section 3.3 - Bart, Dominic, Jan, Javier

Chapter 4: Integration and Design

Sections 4.1 to 4.3 - Daniels, Mikhail

Other

Python scripts - Kamalesh, Sebastien
CATIA Assembly and Part files - Mikhail, Sebastien
CATIA Configurations Model - Dominic
CATIA Technical Drawings - Sebastien
CATIA Kinematic Model - Dominic

Report Finalisation

Chapter 1: Introduction - Javier
Chapter 5: Conclusion & Recommendations - Javier
Chapter : Summary - Bart
Proofreading - All

Hand-in (WP3 Report)